

The method of fundamental solutions applied to boundary eigenvalue problems

Benjamin Bogosel

Abstract

We develop methods based on fundamental solutions to compute the Steklov, Wentzell and Laplace-Beltrami eigenvalues in the context of shape optimization. In the class of smooth simply connected two dimensional domains the numerical method is accurate and fast. A theoretical error bound is given along with comparisons with mesh-based methods. We illustrate the use of this method in the study of a wide class of shape optimization problems in two dimensions. We extend the method to the computation of the Laplace-Beltrami eigenvalues on surfaces and we investigate some spectral optimal partitioning problems.

AMS Subject classifications: 49Q10, 65N80

1 Introduction

The purpose of this article is to provide some tools which facilitate the numerical study of some shape optimization problems. Such problems consist of minimizing or maximizing a certain quantity which depends on the domain geometry. The cost function which is to be optimized may depend on the geometric properties of the domain (perimeter, area) or on some more complex quantities given, for example, by some partial differential equations (eigenvalues, integral energies). Finding explicitly solutions to shape optimization problems may be difficult or even impossible in some cases. Thus, having efficient numerical methods which can allow the study of shape optimization problems is an important issue.

This article treats the numerical optimization of functionals which depend on eigenvalue problems defined on the boundary of the considered domain. The numerical algorithms presented in the sequel allow the computation of the eigenvalues of the Steklov, Wentzell and Laplace-Beltrami spectra. In order to compute these eigenvalues for a given domain we develop a method based on fundamental solutions. This type of methods has been introduced in [32] and has been used by Antunes and Alvez in the study of various eigenvalue problems [2],[3],[4]. The advantage of such a method is the fact that there is no need for a mesh generation at each function evaluation and for a large class of domains the corresponding eigenvalue computation is fast. This fact allows an important time economy if we wish to use the algorithm for numerical shape optimization. Another advantage is that the method based on fundamental solutions is precise. We provide a theoretical result which estimates this error in the case of the Steklov and Wentzell eigenvalues.

There are a few works which present applications of such mesh-less computation methods to the numerical study of shape optimization problems. Among these we mention the minimization of the Laplace Dirichlet eigenvalues by Antunes and Freitas in [6], where the authors also use the method of fundamental solutions. Other functionals depending on the Dirichlet Laplace eigenvalues have been studied by Antunes in [5], using fundamental solutions, and by Osting in [35] using the method of particular solutions for the eigenvalue computation. Optimal convex combinations of Dirichlet Laplace eigenvalues have been studied in [36] and [37] using the MpsPack Matlab toolbox [8] for the eigenvalue computation. In a recent result of Akhmetgaliyev, Kao and Osting [1] the authors provide a numerical method based on a single layer potential in order to compute the Steklov eigenvalues on a two dimensional domain. They also optimize numerically the Steklov eigenvalues under area constraint in dimension two.

We recall that for $\Omega \subset \mathbb{R}^n$ an open set with Lipschitz boundary we can define the **Steklov eigenvalues** as the real values σ for which the following problem has a non trivial solution:

$$\begin{cases} -\Delta u = 0 & \text{in } \Omega, \\ \frac{\partial u}{\partial n} = \sigma u & \text{on } \partial\Omega. \end{cases}$$

It is easy to see that 0 is a Steklov eigenvalue corresponding to constant functions. This problem has a discrete spectrum given by an increasing sequence

$$0 = \sigma_0(\Omega) \leq \sigma_1(\Omega) \leq \sigma_2(\Omega) \leq \sigma_3(\Omega) \leq \dots \rightarrow +\infty$$

As usual, we can provide a variational characterization using Rayleigh quotients

$$\sigma_n(\Omega) = \inf_{S_n} \sup_{u \in S_n \setminus \{0\}} \frac{\int_{\Omega} |\nabla u|^2 dx}{\int_{\partial\Omega} u^2 d\sigma}, \quad n = 1, 2, \dots$$

where S_n is an n dimensional linear subspace of $H^1(\Omega) \cap \{\int_{\partial\Omega} u = 0\}$. This variational formulations allows us to deduce immediately the behaviour of the Steklov eigenvalues under homotheties: $\sigma_k(t\Omega) = \sigma_k(\Omega)/t$ for all $t > 0$.

The study of the Steklov spectrum is and has been a very active field of research. We cite here some notable results concerning the optimization of these eigenvalues. Weinstock proved in [41] that the first non-zero Steklov eigenvalue is maximized by the disk in the class of simply connected two dimensional domains with fixed perimeter. This result was generalized in further directions by Hersch, Payne and Schiffer in [31]. Brock proved in [15] that the first non-zero Steklov eigenvalue is maximized by the ball in every dimension when considering a volume constraint, without any restrictions on the topology of the domain. Other results concerning the optimization of the Steklov spectrum under perimeter constraint are presented in [24]. As underlined in [10], all these optimization results are proved by precisely identifying the optimal shape and then proving that the shape is indeed the desired optimizer. There are cases where the optimal shape cannot be determined explicitly and thus we have a good motivation to develop numerical tools. Concerning the existence of the optimal shapes, some general results are given in [10] in the class of convex sets or the class of sets which satisfy a uniform ε -cone property. General results concerning the existence of optimal shapes for the Steklov problem in the class of simply connected domains can be found in [11].

The **Wentzell spectrum** consists of the real values λ for which the following problem has non-trivial solutions:

$$\begin{cases} -\Delta u = 0 & \text{in } \Omega, \\ -\beta \Delta_{\tau} u + \partial u_n = \lambda u & \text{on } \partial\Omega. \end{cases}$$

We note that the Steklov case corresponds to $\beta = 0$. Although it is possible to study this problem for every real number β , we restrict ourselves to the case $\beta \geq 0$. The Wentzell spectrum is discrete and is given by an increasing sequence denoted

$$0 = \lambda_{0,\beta}(\Omega) \leq \lambda_{1,\beta}(\Omega) \leq \lambda_{2,\beta}(\Omega) \leq \lambda_{3,\beta}(\Omega) \leq \dots \rightarrow +\infty$$

The case of the Wentzell problem has been recently studied in [20] where the authors prove that the ball maximizes locally the first non-zero Wentzell eigenvalue under volume constraint in the class of sets homeomorphic to a ball. It is conjectured that the ball is the global minimizer in the same class of admissible sets. We are able to numerically validate this result in the two dimensional case. We also illustrate the fact that without the topological assumption the conjecture is false.

The second class of problems we study in this article concerns the partitions of a three dimensional surface which minimize the sum of the first Laplace-Beltrami eigenvalues with Dirichlet boundary conditions. It is well known that the **spectrum of Laplace Beltrami operator** with Dirichlet boundary conditions of a subset $\omega \subset \partial\Omega$ consists of the values λ such that the problem

$$\begin{cases} -\Delta_{\tau} u = \lambda u & \text{in } \omega \\ u = 0 & \text{on } \partial\omega \end{cases}$$

has non trivial solutions. This spectrum is discrete and consists of an increasing sequence denoted

$$0 = \lambda_0^{LB}(\omega) \leq \lambda_1^{LB}(\omega) \leq \lambda_1^{LB}(\omega) \leq \dots \rightarrow +\infty.$$

It is known that if ω is homeomorphic to the three dimensional euclidean sphere, then $\lambda_1^{LB}(\omega)$ is maximized by the sphere with the same surface area. For the two dimensional case we know that $\lambda_1^{LB}(\partial\Omega) \leq \lambda_1^{LB}(\partial B)$ where B is a disk of same area as Ω . For a proof of this fact we refer to [20, Section 2.1]. The Wentzell and Laplace-Beltrami eigenvalues are related by the property $\lim_{\beta \rightarrow \infty} \lambda_{k,\beta}(\Omega)/\beta = \lambda_k^{LB}(\partial\Omega)$. For a proof we refer to [20, Section 2.1].

Theoretical aspects concerning this type of partitioning problems, like the questions of existence and regularity, were studied in [18],[27],[28],[29]. The numerical study of this type of partitioning problems is motivated by an open question due to Bishop [9]. It is conjectured that the partition of the sphere into three equal $2\pi/3$ slices minimizes the sum of the fundamental Laplace-Beltrami eigenvalues. One initial objective is to test this conjecture. Previous computations were made by Elliott and Ranner [22] using a penalized formulation introduced in [16]. Their approach allows the study of partitions on various three dimensional surfaces using finite element methods. Our approach is significantly different from theirs and it is related to the computation of the Steklov/Wentzell eigenvalues presented in the first sections of the article. The method we propose uses techniques inspired by [14] along with a refinement procedure in the case of the sphere. Among other methods used in the literature for the study of optimal spectral partitions we cite the rearrangement algorithm used in [38] and the Dirichlet-Neumann approach presented in [12]. The case of the flat torus has been considered in [13]. These works mainly deal with planar partitions or graph partitions. In particular [38] briefly mentions the study of Bishop's conjecture and the expected Y -partition of the sphere is obtained.

The initial part of our optimization procedure uses a phase field formulation where we replace each shape by an approximation of its characteristic function. This gives a rough idea of the structure of the optimal partition. Elliott and Ranner [22] conjectured that the boundaries of the cells are geodesic polygons. In order to test the validity of this fact, we study the problem in the more restrictive class of geodesic polygons. Once we have found the optimal candidates in this restrictive class we add more degrees of freedom to see if the optimal cost decreases. The computation of the Laplace-Beltrami eigenvalues is done using a method based on fundamental solutions. Our numerical results confirm Bishop's conjecture and show that for $n \in \{4, 6, 12\}$ it is likely that the optimal partition is the one associated to the corresponding regular polyhedron. The numerical study of the cases $n \in \{5, 7, 8, 9, 10\}$ as well as a simple argument based on the Gauss-Bonnet formula, shows that, in general, the corresponding optimal partitions do not consist of geodesic polygons.

2 A numerical method for computing the Steklov/Wentzell spectrum

Steklov eigenvalues can be computed numerically using mesh-based methods. This can be done rather quick and in an automatic manner in FreeFem++ [26] and an example code is given in Section 6. Mesh-based methods have the disadvantage that high precision computations need a very fine mesh. On the other hand, as meshes become more and more refined computations become slow. We present below a numerical method which is fast and precise for computing the Steklov spectrum for domains with smooth boundaries.

The method of fundamental solutions, originally introduced in [32], is a part of the class of so called mesh-free numerical methods. This type of method was successfully used in [2],[4] in the study of the eigenvalues of the Dirichlet Laplacian in two and three dimensions. The goal here is to approximate the solution of a problem of the type

$$\begin{cases} Au = 0 \text{ in } \Omega \\ Bu = 0 \text{ on } \partial\Omega, \end{cases} \quad (1)$$

where A, B are suitable linear differential operators. In contrast to methods using meshes, the method of fundamental solutions considers a sufficiently rich class of functions which satisfy $Au = 0$ analytically in

Ω . Thus a linear combination satisfies directly $Au = 0$ in Ω and the coefficients in the linear combination are chosen such that Bu is close to zero on $\partial\Omega$. As we will see in the following, the condition $Bu = 0$ can only be imposed in a finite number of points, so the condition $Bu = 0$ will be satisfied only in an approximate manner on $\partial\Omega$. To justify our numerical approach, an error bound is provided in Section 3, which basically says that if Bu is small enough, then u is close to the real solution.

In our case, the operator A is the Dirichlet Laplacian and the operator B is given by $-\beta\Delta_\tau + \frac{\partial}{\partial n} - \lambda\text{Id}$, where Δ_τ is the Laplace-Beltrami operator associated to $\partial\Omega$. Our set of fundamental solutions consists of harmonic, radial functions, with centers outside Ω . In this way, any linear combination of such functions solves $\Delta u = 0$ in Ω . The only thing we need to do is to find the right coefficients so that the condition $-\beta\Delta_\tau u + \frac{\partial u}{\partial n} = \lambda u$ is satisfied on $\partial\Omega$. In order to compute the expression of the Laplace-Beltrami operator on $\partial\Omega$ we use the formula

$$\Delta u = \Delta_\tau u + \mathcal{H} \frac{\partial u}{\partial n} + \frac{\partial^2 u}{\partial n^2},$$

which is valid on $\partial\Omega$. We have used the notation $\frac{\partial^2 u}{\partial n^2}$ to denote $(D^2 u \cdot n) \cdot n$. As usual, \mathcal{H} denotes the mean curvature of $\partial\Omega$. For more details we refer to [30, Chapter 5].

In $\mathbb{R}^2 \setminus \{0\}$ a radial solution of the Laplace equation is given by $\phi(x) = \ln|x|$. Note that this solution has a singularity at $x = 0$. For every $y \in \mathbb{R}^2$ the function $\psi_y(x) = \phi(x - y)$ is harmonic in $\mathbb{R}^2 \setminus \{y\}$ and radial with center y . Given $\Omega \subset \mathbb{R}^2$ we choose $y_1, \dots, y_N \in \mathbb{R}^2 \setminus \Omega$ and $x_1, \dots, x_N \in \partial\Omega$. The function $x \mapsto \alpha_1 \psi_{y_1}(x) + \dots + \alpha_N \psi_{y_N}(x)$ is harmonic in Ω for every choice of the coefficients $(\alpha_i)_{i=1}^N$. We impose for $i = 1 \dots N$ the boundary condition

$$\left(-\beta\Delta_\tau + \frac{\partial}{\partial n}\right) (\alpha_1 \psi_{y_1}(x_i) + \dots + \alpha_N \psi_{y_N}(x_i)) = \sigma (\alpha_1 \psi_{y_1}(x_i) + \dots + \alpha_N \psi_{y_N}(x_i)) \quad (2)$$

This amounts to solve a generalized eigenvalue problem for square matrices.

In this setting, it is straightforward to find the first eigenvalues corresponding to the generalized eigenvalue problem determined by (2), using, for example the `eigs` solver in Matlab. One of the main difficulties is the choice of the points $(x_i)_{i=1}^N, (y_i)_{i=1}^N$. As noted in [2], an arbitrary choice for $(x_i), (y_i)$ may fail to give a valid approximate solution for the desired eigenvalue problem. We notice the same behaviour and we discuss below our choice of the points $(x_i), (y_i)$.

We tested two choices for the points (x_i) . The first one consists in taking a uniform division (θ_i) of $[0, 2\pi]$ into N intervals and then choose $x_i = \rho(\theta_i)(\cos \theta_i, \sin \theta_i)$, where ρ is the radial function which parametrizes $\partial\Omega$. A second choice is choosing x_i at equal arclength distances on the boundary $\partial\Omega$. We did not observe major differences between the two choices of points mentioned above. From a computational point of view the uniform angle choice is faster. The method based on equal arclength distances may improve the behaviour of the algorithm if the domain is thin or if the radial function has large oscillations. Having chosen (x_i) , we can compute the corresponding outer normals (\vec{n}_i) and we define $y_i = x_i + c \cdot \vec{n}_i$. In our computations we choose $c = 0.1$.

The choice of this factor is important in the computations. Although the value $c = 0.1$ has been initially found experimentally, we give an argument which supports this choice. We note that as the distance to the boundary increases the conditioning number of the matrices involved in the generalized eigenvalue problem (2) increases. On the contrary, as the source points come close to the boundary, the problem becomes singular. Values of the distance close to 0.1 give a good balance for the conditioning number and the numerical errors generated by the method. This optimal distance c depends only on the choice of the fundamental solutions.

It is not hard to see the limitations of this method. Since linear combinations of fundamental solutions have singularities at their source points, it is clear that these source points must be located outside the computation domain. Another aspect is that source points must be distinct so that equations (2) do not repeat themselves. These two aspects already suggest that domains with cusps or re-entrant parts are not covered by our algorithm.

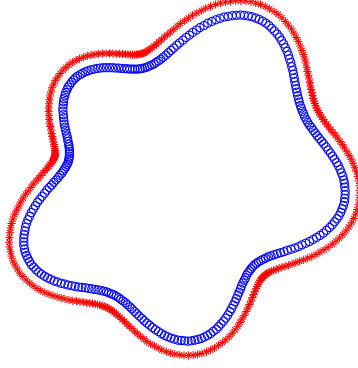


Figure 1: The position of the source points and the evaluation points for the shape given by the radial parametrization 7 with Fourier coefficients equal to $[1, 0.1, 0, 0, 0, 0.1, 0, 0.1, 0, 0, -0.1]$.

3 Error estimates

In the case of the Dirichlet Laplacian, the result proved by Moler and Payne in [33], states that if a function u satisfies $-\Delta u = \lambda u$ in Ω and u is sufficiently small on $\partial\Omega$ then λ is close to an eigenvalue of the Dirichlet-Laplace operator associated to Ω . We provide a similar result below in the case of the Wentzell eigenvalue problem, which helps validate our numerical computations. In the following paragraphs we assume that Ω has Lipschitz boundary and that it has finite perimeter. In the following we denote $V(\partial\Omega) = \{u \in L^2(\partial\Omega) : \int_{\partial\Omega} u = 0\}$.

As in [20] we introduce the Hilbert space $H(\Omega) = \{u \in H^1(\Omega) : \text{Tr}(u) \in H^1(\partial\Omega), \int_{\partial\Omega} u = 0\}$ where Tr is the trace operator. In the case $\beta = 0$ it suffices to take $H(\Omega) = H^1(\Omega)$. Consider for $f \in V(\partial\Omega)$ the minimization problem

$$\min_{u \in H(\Omega)} \frac{1}{2} \left(\int_{\Omega} |\nabla u|^2 + \beta \int_{\partial\Omega} |\nabla_{\tau} u|^2 \right) - \int_{\partial\Omega} u f$$

which has a unique solution. This solution satisfies the weak formulation

$$\int_{\Omega} \nabla u \cdot \nabla \varphi + \beta \int_{\partial\Omega} \nabla_{\tau} u \nabla_{\tau} \varphi = \int_{\partial\Omega} f \varphi, \quad \forall \varphi \in C^1(\bar{\Omega}), \quad (3)$$

of the partial differential equation

$$\begin{cases} -\Delta u = 0 & \text{in } \Omega \\ -\beta \Delta_{\tau} u + \frac{\partial u}{\partial n} = f & \text{on } \partial\Omega, \end{cases} \quad (4)$$

where Δ_{τ} is the Laplace-Beltrami operator and ∇_{τ} is the tangential gradient associated to $\partial\Omega$. Thus, we can define the resolvent operator $R_{\beta} : L^2(\partial\Omega) \rightarrow H(\Omega)$ associated to this equation. The trace operator $T : H(\Omega) \rightarrow V(\partial\Omega)$ being continuous it follows that the operator $T \circ R_{\beta} : V(\partial\Omega) \rightarrow V(\partial\Omega)$ is compact and injective. We can define its inverse $A_{\beta} : D(A_{\beta}) \subset V(\partial\Omega) \rightarrow V(\partial\Omega)$. Since $T \circ R_{\beta}$ is a compact operator, the spectrum of the operator A_{β} consists of an increasing sequence of non-negative eigenvalues $\lambda_{k,\beta}(\Omega)$ which diverges. The corresponding eigenfunctions form a Hilbert basis for $V(\partial\Omega)$. By considering the constant function 1 associated to the zero eigenvalue of this operator, we can say that the set of eigenvalues forms a Hilbert basis of $L^2(\partial\Omega)$. The following result proves that the operator $T \circ R_{\beta}$ is bounded and gives an idea of how to find its norm. To simplify the proofs we denote the trace of a function $w \in H^1(\Omega)$ by w .

Proposition 3.1. *Let Ω be a bounded, open domain with Lipschitz boundary. Suppose $f \in V(\partial\Omega)$ and $w = R_{\beta} f \in H^1(\Omega)$. Then there exists a constant C , depending only on Ω , such that*

$$\|w\|_{L^2(\partial\Omega)} \leq C \|f\|_{L^2(\partial\Omega)}.$$

Proof: The trace inequality (Chapter 4.3 [23]) for Ω implies the existence of a constant C_1 (depending only on Ω) such that $\|u\|_{L^2(\partial\Omega)} \leq C_1\|u\|_{H^1(\Omega)}$ for every $u \in H^1(\Omega)$. The Poincaré-Wirtinger inequality implies the existence of a constant C_2 which depends only on Ω such that $\|\tilde{w}\|_{L^2(\Omega)} \leq C_2\|\nabla w\|_{L^2(\Omega)}$, where $\tilde{w} = w - \frac{1}{|\Omega|}\|w\|_{L^2(\Omega)}$. The weak formulation of the equation $R_\beta f = w$ and the Cauchy-Schwarz inequality imply that

$$\int_{\Omega} |\nabla \tilde{w}|^2 + \beta \int_{\partial\Omega} |\nabla_\tau \tilde{w}|^2 = \int_{\partial\Omega} f \tilde{w} \leq \|f\|_{L^2(\partial\Omega)} \|\tilde{w}\|_{L^2(\partial\Omega)}.$$

Using the remarks above, we obtain

$$\|\tilde{w}\|_{L^2(\partial\Omega)}^2 \leq C_1^2(\|\tilde{w}\|_{L^2(\Omega)}^2 + \|\nabla \tilde{w}\|_{L^2(\Omega)}^2) \leq C_1^2(1 + C_2^2)\|\nabla \tilde{w}\|_{L^2(\Omega)}^2.$$

Thus

$$\|\tilde{w}\|_{L^2(\partial\Omega)}^2 \leq C_1^2(1 + C_2^2)\|f\|_{L^2(\partial\Omega)} \|\tilde{w}\|_{L^2(\partial\Omega)},$$

which implies

$$\|\tilde{w}\|_{L^2(\partial\Omega)} \leq C_1^2(1 + C_2^2)\|f\|_{L^2(\partial\Omega)}.$$

On the other hand, since w has average 0 on $\partial\Omega$, we know that the $L^2(\partial\Omega)$ norm of $w + c$ is minimal when $c = 0$ (here c is a constant). Therefore

$$\|w\|_{L^2(\partial\Omega)} \leq \|\tilde{w}\|_{L^2(\partial\Omega)} \leq C_1^2(1 + C_2^2)\|f\|_{L^2(\partial\Omega)}.$$

□

The constants C_1, C_2 can be found explicitly in terms of the domain Ω . The constant C_1 depends on the Lipschitz constant of Ω and $C_2 = 1/\lambda_1(\Omega)$, where $\lambda_1(\Omega)$ is the first eigenvalue of the Dirichlet Laplacian operator on Ω . These quantities may be evaluated on particular domains and together with the result presented below can provide an exact error estimate.

Using ideas similar to the ones used by Moler and Payne in [33], we are able to prove the following error estimate. For simplicity of notation we omit the reference to β from R_β .

Theorem 3.2. *Consider Ω a bounded, open domain with Lipschitz boundary and finite perimeter. Suppose that u_ε satisfies the following approximate eigenvalue problem:*

$$\begin{cases} -\Delta u_\varepsilon = 0 & \text{in } \Omega \\ -\beta \Delta_\tau u_\varepsilon + \frac{\partial u_\varepsilon}{\partial n} = \lambda_\varepsilon u_\varepsilon + f_\varepsilon & \text{on } \partial\Omega. \end{cases} \quad (5)$$

Denote $w_\varepsilon = Rf_\varepsilon$. Let $\delta = \frac{\|w_\varepsilon\|_{L^2(\partial\Omega)}}{\|u_\varepsilon\|_{L^2(\partial\Omega)}}$ and suppose that $\delta < 1$. Then there exists a Wentzell eigenvalue λ_k satisfying

$$\frac{|\lambda_\varepsilon - \lambda_k|}{\lambda_k} \leq \delta.$$

Proof: We know that there exists a Hilbert basis of $L^2(\partial\Omega)$ formed of Wentzell eigenfunctions u_n corresponding to the Wentzell eigenvalues λ_n of Ω . We denote the standard scalar product in $L^2(\partial\Omega)$ by $(u, v) = \int_{\partial\Omega} uv$. Let $a_n = (u_\varepsilon, u_n)$, $b_n = (w_\varepsilon, u_n)$. We know that $R(\lambda_\varepsilon u_\varepsilon + f_\varepsilon) = u_\varepsilon$ and $Ru_n = u_n/\lambda_n$. The resolvent operator R is symmetric, thus

$$\begin{aligned} a_n &= (u_\varepsilon, u_n) = (R(\lambda_\varepsilon u_\varepsilon + f_\varepsilon), u_n) \\ &= (\lambda_\varepsilon u_\varepsilon, Ru_n) + (Rf_\varepsilon, u_n) \\ &= \frac{\lambda_\varepsilon}{\lambda_n} (u_\varepsilon, u_n) + (w_\varepsilon, u_n) \\ &= \frac{1}{\lambda_n} (\lambda_\varepsilon a_n + \lambda_n b_n). \end{aligned}$$

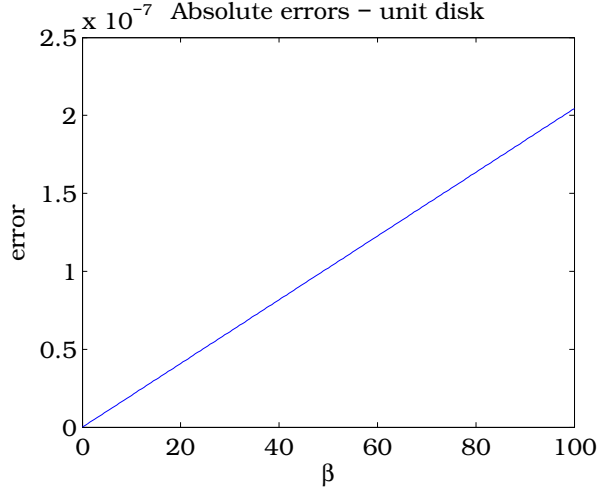


Figure 2: Difference between the computed eigenvalues and the analytic eigenvalues on the unit disk. The parameter β is taken on a discretization of $[0, 100]$ with step 0.1.

Thus, for every n we have $\frac{\lambda_n - \lambda_\varepsilon}{\lambda_n} = \frac{b_n}{a_n}$. Since $\lambda_n \rightarrow \infty$ as $n \rightarrow \infty$, there exists an index k such that

$$\frac{|\lambda_k - \lambda_\varepsilon|}{|\lambda_k|} = \min_{n \in \mathbb{N}^*} \frac{|\lambda_n - \lambda_\varepsilon|}{|\lambda_n|}.$$

For this index k we have

$$\frac{|\lambda_k - \lambda_\varepsilon|}{|\lambda_k|} |a_n| \leq |b_n|,$$

for all n and

$$\frac{|\lambda_k - \lambda_\varepsilon|^2}{|\lambda_k|^2} \sum_{n=1}^{\infty} a_n^2 \leq \sum_{n=1}^{\infty} b_n^2.$$

This is exactly

$$\frac{|\lambda_k - \lambda_\varepsilon|}{|\lambda_k|} \leq \delta,$$

which finishes the proof. \square

The only hypothesis in the above theorem which needs to be verified in order to apply it in our case is that we can solve the partial differential equation $w_\varepsilon = R_\beta f_\varepsilon$ in the case where f_ε is a combination of the fundamental solutions. As we have seen the necessary and sufficient condition is $\int_{\partial\Omega} f_\varepsilon = 0$. Note that this condition can always be satisfied by adding a constant function to the family of fundamental solutions.

4 Testing the numerical method

There are few shapes for which the Wentzell spectrum is known analytically. One such shape is the unit disk D_1 , for which the eigenvalues are

$$\lambda_{k,\beta}(D_1) = \left\lfloor \frac{k+1}{2} \right\rfloor + \beta \left\lfloor \frac{k+1}{2} \right\rfloor^2.$$

As an initial test for our algorithm we compute the Wentzell spectrum of the disk for $N = 300$ points on ∂D_1 and 300 corresponding fundamental solutions. For $\beta = 0$ we have 10 digits of precision for the first 10 eigenvalues. In Figure 2 we plot the absolute error for the first 10 Wentzell eigenvalues, given by

$\max_{i=1}^{10} |\lambda_{k,\beta}(D_1) - \tilde{\lambda}_{k,\beta}(D_1)|$, for $\beta \in [0, 100]$. We denoted $\tilde{\lambda}_{k,\beta}$ the numerically computed eigenvalue. We note that for $\beta = 100$ we still have 6 digits of precision.

In order to test our algorithm for shapes for which no analytical expression is known for the Wentzell eigenvalues, we use FreeFem++ [26], which is a mesh-based method. The tests we performed show that our results are in good correspondence with the values found with FreeFem++. The downside of the mesh-based method is the execution time, which is significantly more important when the number of mesh triangles is high. An example of implementation is presented in Section 6. In Tables 1, 2, 3 we compare the Wentzell eigenvalues computed with our method (MFS) and the ones obtained with FreeFem++. As a test case we take the shape given in Figure 1, for various values of β . Note that as the number of triangles increases, the values computed with the FreeFem++ method approach the values found with our algorithm. We underline the fact that our algorithm runs in approximately 0.1 seconds¹, whereas the FreeFem++ algorithm, with over 450000 triangles takes about a minute on the same machine.

This method of fundamental solutions can be adapted to compute the Laplace-Beltrami spectrum of a closed simple curve in \mathbb{R}^2 . We can consider solving the equation

$$\Delta_\tau(\alpha_1\psi_{y_1}(x_i) + \dots + \alpha_N\psi_{y_N}(x_i)) = \lambda(\alpha_1\psi_{y_1}(x_i) + \dots + \alpha_N\psi_{y_N}(x_i)), \quad i = 1 \dots N \quad (6)$$

which also leads to a generalized eigenvalue problem. The Laplace-Beltrami spectrum of a one dimensional curve depends only on its length and is given by $\lambda_k = \lfloor \frac{k+1}{2} \rfloor^2 \left(\frac{2\pi}{L}\right)^2$. The method of fundamental solutions computes these values with a relative error of order 10^{-7} (with the same parameters: 300 boundary points and exterior points at distance 0.1 of the boundary). This good behaviour motivates the extension of the method to the computation of Laplace-Beltrami eigenvalues for subsets of the the unit sphere, presented in Section 7.

We may use Theorem 3.2 in order to have a quantitative evaluation of the error on a general domain. The result cited above states that the relative error made in the numerical computations is of order $\|f_\varepsilon\|_{L^2(\partial\Omega)}$, where f_ε is the error term in (5). We may estimate numerically f_ε as follows: given a shape Ω , we compute its Steklov/Wentzell eigenvalues with the algorithm presented in previous sections. We know that the eigenvalue equation is satisfied to machine precision on the discretization points chosen on $\partial\Omega$. In order to have a more precise evaluation of what happens between these points we make a refinement by placing 100 supplementary points between every two discretization points. We evaluate f_ε in each of these points. The maximal value found for f_ε gives us an estimate of the general error. Below you can see plots of f_ε for the first 10 eigenvalues in three different cases. By looking at the maximal errors, we can observe that $\|f_\varepsilon\|_{L^2(\partial(\Omega))}$ is of order 10^{-6} or smaller. As expected, different domains give different behaviours and the precision can be much higher in some particular cases.

5 Numerical optimization of functionals depending on the Wentzel spectrum

Using the computational method presented in the previous sections we can study numerically some shape optimization problems regarding the Wentzell spectrum in the particular case of star-shaped domains. We consider domains parametrized by their radial functions $\rho : [0, 2\pi) \rightarrow \mathbb{R}_+$. We approximate ρ by the truncation of its Fourier series to $2n + 1$ coefficients:

$$\rho(\theta) \approx a_0 + \sum_{i=1}^n a_i \cos(i\theta) + \sum_{i=1}^n b_i \sin(i\theta). \quad (7)$$

In this way we have an approximation of $\sigma_k(\Omega)$ using a finite number of parameters. Using the shape derivative formula provided in [20, Section E] (see also [1]) we can deduce that

$$\frac{\partial \lambda_{k,\beta}}{\partial a_i} = \int_0^{2\pi} (|\nabla_\tau u_k|^2 - |\partial_n u_k|^2 - \lambda_{k,\beta} \mathcal{H}|u_k|^2 + \beta(\mathcal{H}I - 2D^2b)\nabla_\tau u_k \cdot \nabla_\tau u_k) \rho(\theta) \cos(i\theta) d\theta$$

¹Machine configuration: 2.2 Ghz quad-core i7 processor, 6 Gb RAM memory

	our algorithm	FreeFem++ (refined meshes)			
k	MFS	19146 ▲	53236 ▲	211290▲	474634▲
1	0.712751	0.712989	0.712837	0.712773	0.712761
2	0.940247	0.940538	0.940352	0.940274	0.940259
3	1.381278	1.38211	1.38158	1.38135	1.38131
4	1.443204	1.44411	1.44353	1.44329	1.44324
5	3.146037	3.14712	3.14643	3.14614	3.14608
6	3.443637	3.44496	3.44411	3.44376	3.44369
7	3.757833	3.761	3.75897	3.75812	3.75796
8	3.922821	3.9263	3.92407	3.92313	3.92296
9	4.274362	4.28034	4.27651	4.2749	4.2746
10	4.693206	4.70035	4.69578	4.69385	4.6935

Table 1: Comparison with FreeFem++, $\beta = 0$ (Steklov) for the shape given in Figure 1

	our algorithm	FreeFem++ (refined meshes)			
k	MFS	19146 ▲	53236 ▲	211290▲	474634▲
1	2.375744	2.37628	2.37594	2.37579	2.37577
2	2.644741	2.6453	2.64494	2.64479	2.64476
3	8.042223	8.04527	8.04332	8.0425	8.04234
4	8.257585	8.26043	8.25861	8.25784	8.2577
5	16.909967	16.9197	16.9135	16.9108	16.9104
6	17.383930	17.3932	17.3873	17.3848	17.3843
7	28.883924	28.9094	28.8931	28.8862	28.8849
8	29.113307	29.1374	29.122	29.1155	29.1143
9	43.718607	43.77	43.7371	43.7232	43.7207
10	44.142742	44.1996	44.1632	44.1479	44.145

Table 2: Comparison with FreeFem++, $\beta = 2$ for the shape given in Figure 1

	our algorithm	FreeFem++ (refined meshes)			
k	MFS	19146 ▲	53236 ▲	211290▲	474634▲
1	4.750048	4.75121	4.75047	4.75015	4.75009
2	5.02106	5.02224	5.02148	5.02117	5.02111
3	17.557103	17.5638	17.5595	17.5577	17.5574
4	17.774667	17.781	17.777	17.7752	17.7749
5	38.179237	38.2016	38.1873	38.1812	38.1801
6	38.65575	38.6771	38.6634	38.6577	38.6566
7	66.764114	66.8228	66.7852	66.7694	66.7665
8	66.995238	67.0507	67.0152	67.0002	66.9975
9	102.91875	103.038	102.962	102.929	102.924
10	103.34252	103.474	103.39	103.354	103.348

Table 3: Comparison with FreeFem++, $\beta = 5$ for the shape given in Figure 1

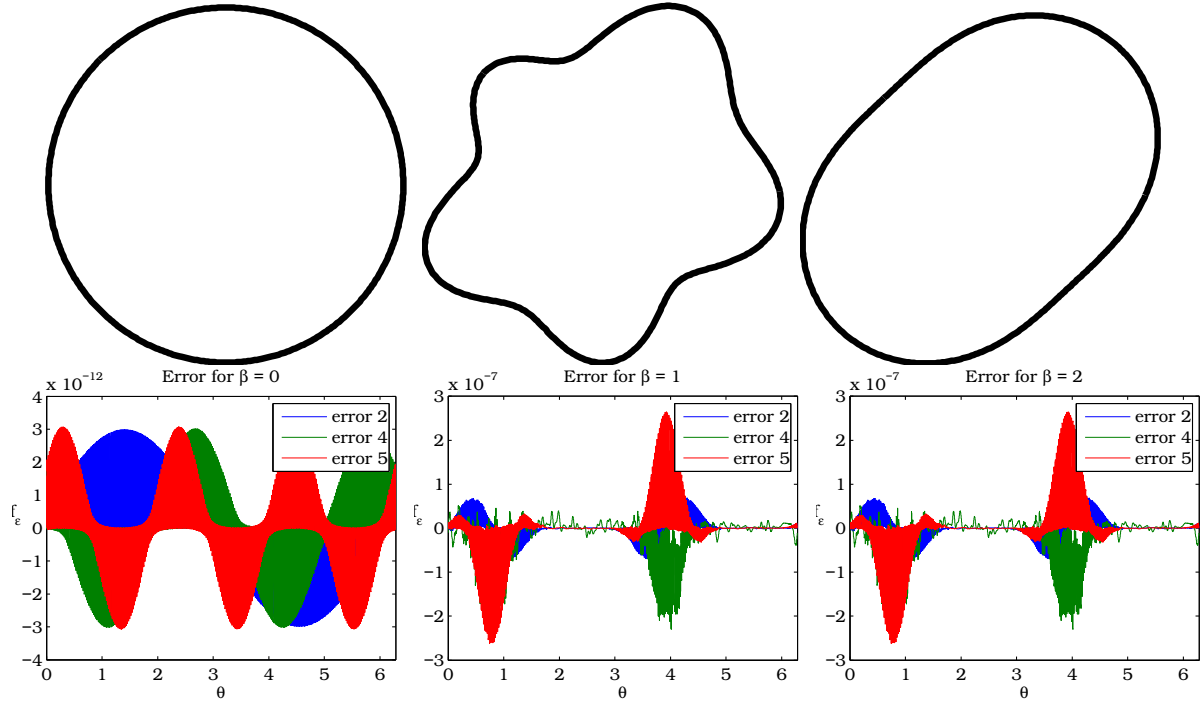


Figure 3: Graph of the error term in the computation of the Steklov and Wentzell eigenvalues of indexes $k = 2, 4, 5$ (various values of β).

and

$$\frac{\partial \lambda_{k,\beta}}{\partial b_i} = \int_0^{2\pi} (|\nabla_\tau u_k|^2 - |\partial_n u_k|^2 - \lambda_{k,\beta} \mathcal{H}|u_k|^2 + \beta(\mathcal{H}I - 2D^2b)\nabla_\tau u_k \cdot \nabla_\tau u_k) \rho(\theta) \sin(i\theta) d\theta$$

We use the notation \mathcal{H} for the mean curvature of $\partial\Omega$. We denote by D^2b the hessian of the signed distance function b . We have denoted u_k the eigenfunction corresponding to $\lambda_{k,\beta}(\Omega)$ normalized in $L^2(\partial\Omega)$.

Since we can approximate $\lambda_{k,\beta}(\Omega)$ by a function $\lambda_{k,\beta}(a_0, a_1, \dots, a_n, b_1, \dots, b_n)$ for which we know the gradient with respect to every component, we can use a gradient descent algorithm for solving different optimization problems related to the Wentzell eigenvalues. This kind of approach is well known and was used in [35] and [6] for optimizing functionals of the eigenvalues of the Dirichlet Laplacian and also in [1] in the case of the Steklov eigenvalues. The Steklov eigenvalue behaves well under homotheties, so in order to optimize under area or perimeter constraint we can just optimize the normalized quantities $\sigma_k(\Omega)|\Omega|^{1/2}$, $\sigma_k(\Omega) \text{Per}(\Omega)$. In the Wentzell case, $\beta > 0$, we do not have this property. In order to preserve the constraint we simply rescale the shape after each iteration in the gradient descent algorithm in order to have the desired area or perimeter.

The only part which poses some difficulty in the implementation is finding a way to efficiently compute the normal and tangential components of u_k . We present below the main lines of the computational algorithm. An example of such computation algorithm can be consulted on the author's webpage. ²

- Choose the number of discretization points (in our case $N = 300$) and find the derivatives of the radial function, namely ρ, ρ', ρ'' , evaluated at each corresponding point. Note that this can be done analytically and all we need to do in the end is to write some matrix vector products.
- With the aid of the derivatives of ρ we can construct the exterior normals

$$\vec{n}(\theta) = (\rho(\theta) \cos \theta + \rho'(\theta) \sin \theta, \rho(\theta) \sin \theta - \rho'(\theta) \cos \theta) / \sqrt{\rho(\theta)^2 + \rho'(\theta)^2},$$

the curvature \mathcal{H} and the hessian of the signed distance function D^2b (as the differential of the normal defined as above).

²http://www.lama.univ-savoie.fr/~bogose1/software/wentzell_test.m

- With the aid of the normals we construct the exterior points and we write the generalized eigenvalue problem 2.
- We solve the respective generalized eigenvalue problem with the algorithm `eigs` in Matlab and we recover the corresponding eigenvector. This eigenvector contains the coefficients in the linear combination of fundamental solutions

$$u_k = \sum_{i=1}^N \alpha_i \psi_i$$

- We compute analytically the gradient of u_k and then we compute the tangential and normal components needed in the computation of the derivative. In order to do this we need to find the gradient and the hessian of each fundamental solution analytically. This is straightforward, given the formulas $\psi_i = \ln |x - y_i|$.
- We use a basic quadrature rule for the normalization of the eigenvalues and for the computation of the integrals needed to express the gradient.

As a test for our algorithm we perform some numerical optimization procedures for some problems with known optimizers. There are many such results for the case of the Steklov eigenvalue problem given by $\beta = 0$. We use the notation σ_k for the Steklov eigenvalues, corresponding to $\lambda_{k,0}$. We start from a random shape in order to avoid local minima. We mention that all computations are made in the class of simply connected sets. We were able to test our algorithm in the following cases:

- $\max \sigma_1(\Omega)$ is achieved when Ω is a disk, in the case of perimeter and area constraints ([41],[15]);
- $\max \sigma_1(\Omega)\sigma_2(\Omega)$ is achieved when Ω is a disk, in the case of perimeter and area constraints ([31]);
- $\min \sum_{k=1}^n \frac{1}{\sigma_k(\Omega)}$ is achieved when Ω is a disk, in the case of perimeter and area constraints [31]);
- $\max \sigma_k(\Omega)$ for domains which are invariant under a rotation of angle $2\pi/q$ ($q > 1$) is achieved by a disk in the case of the perimeter constraint ([7]).

In the article of Dambrine, Lamboley and Kateb [20], the authors prove that the ball is a local maximizer for the first non-zero Wentzel eigenvalue if $\beta \geq 0$, under volume constraint in the class of sets homeomorphic to the ball. In the same article it is proved that $\lambda_{1,\beta}(B_R) = (d-1)\beta/R^2 + 1/R$ which is decreasing with respect to R . Here we denote B_R the ball of radius R in \mathbb{R}^d . In the following we denote by \mathcal{A} a class of sets in \mathbb{R}^d which contains all balls. We can deduce the following property.

Proposition 5.1. *If $\lambda_{1,\beta}(\Omega)$ is maximized by the ball in \mathcal{A} under perimeter constraint, then $\lambda_{1,\beta}$ is also maximized by the ball in the same class, under volume constraint.*

Proof. Let $\Omega \in \mathcal{A}$ and denote B_p, B_v the balls with the same perimeter and the same volume as Ω , respectively. Suppose $\lambda_{1,\beta}(\Omega) \leq \lambda_{1,\beta}(B_p)$. The isoperimetric inequality implies that $\text{Per}(B_p) = \text{Per}(\Omega) \geq \text{Per}(B_v)$ and thus B_v has smaller radius than B_p . The monotonicity of the first Wentzell eigenvalue with respect to the radius of the ball implies that

$$\lambda_{1,\beta}(\Omega) \leq \lambda_{1,\beta}(B_p) \leq \lambda_{1,\beta}(B_v).$$

This chain of inequalities shows that if $\lambda_{1,\beta}$ is maximized by the ball under perimeter constraint in the class \mathcal{A} then the ball is also a maximizer in the same class, but under a volume constraint. \square

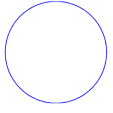

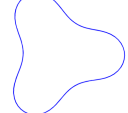

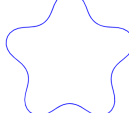
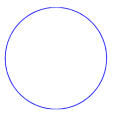
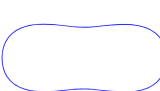
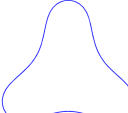
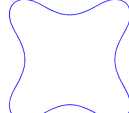

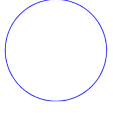
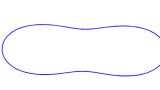
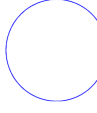
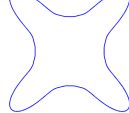
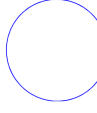
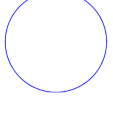
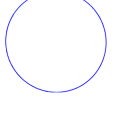
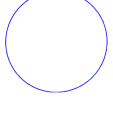
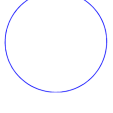
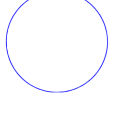
	λ_1	λ_2	λ_3	λ_4	λ_5
$\beta = 0$ (Steklov)	 $\lambda_1 = 1$	 $\lambda_2 = 1.64$	 $\lambda_3 = 2.33$	 $\lambda_4 = 2.97$	 $\lambda_5 = 3.66$
$\beta = 0.1$	 $\lambda_1 = 1.1$	 $\lambda_2 = 1.80$	 $\lambda_3 = 2.65$	 $\lambda_4 = 3.42$	 $\lambda_5 = 4.3$
$\beta = 0.5$	 $\lambda_1 = 1.5$	 $\lambda_2 = 2.39$	 $\lambda_3 = 4$	 $\lambda_4 = 4.53$	 $\lambda_5 = 7.5$
$\beta = 100$ (large)	 $\lambda_1 = 101$	 $\lambda_2 = 101$	 $\lambda_3 = 402$	 $\lambda_4 = 402$	 $\lambda_5 = 903$

Table 4: Numerical maximizers for the first five Wentzell eigenvalues for different values of β . The areas of the domains are equal to π

It is a well known fact, due to Weinstock [41] and Brock [15], that when $\beta = 0$ the ball is the optimizer for both volume and perimeter constraints with the difference that Weinstock's result requires that the domain is simply connected, while Brock's result is independent of the topology. Using our algorithm, we search for the shape which optimizes $\lambda_{1,\beta}(\Omega)$ in two dimensions. For both perimeter and area constraints we obtained that the disk is the numerical maximizer of $\lambda_{1,\beta}$ among two dimensional simply connected shapes. We performed tests for $\beta \in [0, 100]$, but we believe it to be true for every $\beta > 0$ since for large values of β , $\lambda_{1,\beta}(\Omega)/\beta$ converges to the first Laplace-Beltrami eigenvalue of $\partial\Omega$, which is also maximized by the disk in the same class of domains. We also perform tests in the case of the area constraint for $k = 2, 3, 4, 5$ and we present the results in Table 4. For large β we observe that the optimal shapes are close to a disk, which is the expected behaviour, as we know that the disk maximizes the Laplace-Beltrami eigenvalues of $\partial\Omega$ when Ω has fixed area.

We also perform some numerical optimizations for problems inspired from known results for the Steklov spectrum. These computations suggest that the conjectures stated below are valid. These results are obtained in the class of domains which are simply connected and star-shaped.

- $\max \lambda_{1,\beta}(\Omega)$ is achieved by the disk;

- $\min \sum_{k=1}^n \frac{1}{\lambda_{k,\beta}(\Omega)}$ is achieved by the disk;

- We say that $A \subset \{0, 1, 2, 3, \dots\}$ has the property (P) if $1 \in A$ and $2k \in A \Rightarrow 2k - 1 \in A$. If A has the property (P) then $\sum_{k \in A} \frac{1}{\lambda_{k,\beta}(\Omega)}$ is minimized by the disk in the case of a area and perimeter constraint. For example $\frac{1}{\lambda_{1,\beta}(\Omega)} + \frac{1}{\lambda_{3,\beta}(\Omega)} + \frac{1}{\lambda_{4,\beta}(\Omega)}$ is minimized by the disk in the case of the area constraint and the perimeter constraint. This was verified for various sets A with property (P)

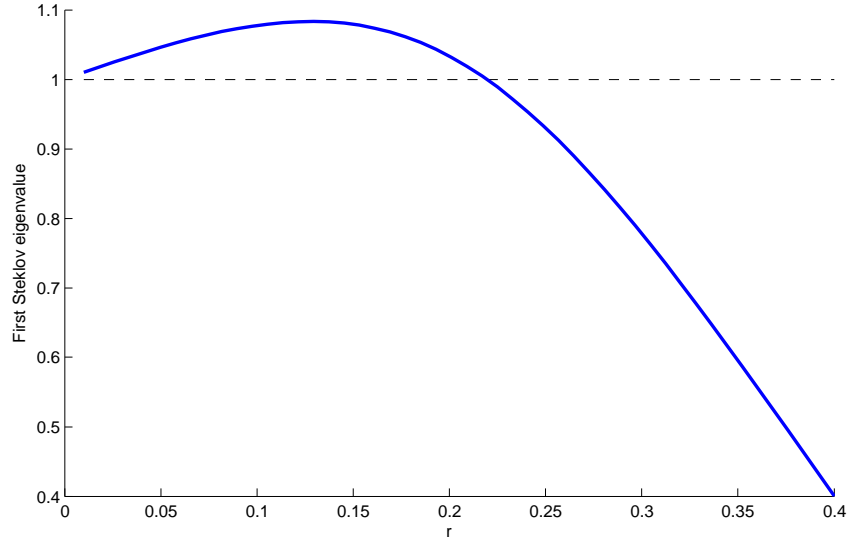


Figure 4: The first Steklov eigenvalues of an annulus with perimeter 2π and inner radius r is plotted as a function of r .

with $A \subset \{0, 1, \dots, 15\}$. We note that this conjecture is not proved even in the case of the Steklov eigenvalues.

We note that if Ω is a two dimensional domain then all these numerical observations are seen to be valid as $\beta \rightarrow \infty$. Indeed, in this case $\partial\Omega$ is a one-dimensional contour, and its corresponding Laplace-Beltrami eigenvalues are proportional to $1/L^2$ where L is the perimeter of Ω . Thus all the above optimization problems, in the Laplace-Beltrami case, have the disk as a solution, under area constraint, as a simple consequence of the classical isoperimetric inequality.

As underlined before, when considering a perimeter constraint, the simple connectedness is essential for the optimality of the disk for the first Steklov eigenvalue. The initial proof in [41] uses the fact that $\partial\Omega$ is a simple closed curve. Techniques from [31], using conformal mappings, can also be used to prove the same result, but again the constraint on the topology is essential. If we remove this constraint, the result is no longer valid. In [25, Section 4.2] the authors show that there are annuli with same perimeter but with the first Steklov eigenvalue greater than the corresponding eigenvalue on the disk. This behaviour can be seen in Figure 4 in some computations made with FreeFem++. We consider the annuli with fixed perimeter 2π bounded by two circles of radii r and $R = 1 - r$ and we plot the corresponding first Steklov eigenvalue as a function of r . As proved by Brock [15], if we consider instead an area constraint then the simple connectedness condition is not necessary. Indeed, Brock uses a classical variational characterization of the sum of the inverses of the first d eigenvalues. In this variational characterization he takes as test functions the first d Steklov eigenvalues on the disk, which are made admissible by making a suitable translation of the domain. As a final ingredient, a weighted isoperimetric inequality shows that

$$\sum_{i=1}^d \frac{1}{\sigma_i(\Omega)} \geq \sum_{i=1}^d \frac{1}{\sigma_i(B)}, \quad |B| = |\Omega|.$$

The fact that the first d eigenvalues on the ball B are equal implies that $\sigma_1(\Omega) \leq \sigma_1(B)$. We may ask if in the case for the Wentzell eigenvalues we can remove the topology constraint as well. The answer is negative, as can be seen in Figure 5 for $\beta \in \{0.1, 0.2, 0.3\}$. We consider annuli of fixed area π bounded by circles of radius r and $R = \sqrt{1+r^2}$. We present the graphs of the first Wentzell eigenvalue as function of r and we note that for $\beta > 0$ there are annuli with the same area as the unit disk, but with higher first Wentzell eigenvalues.

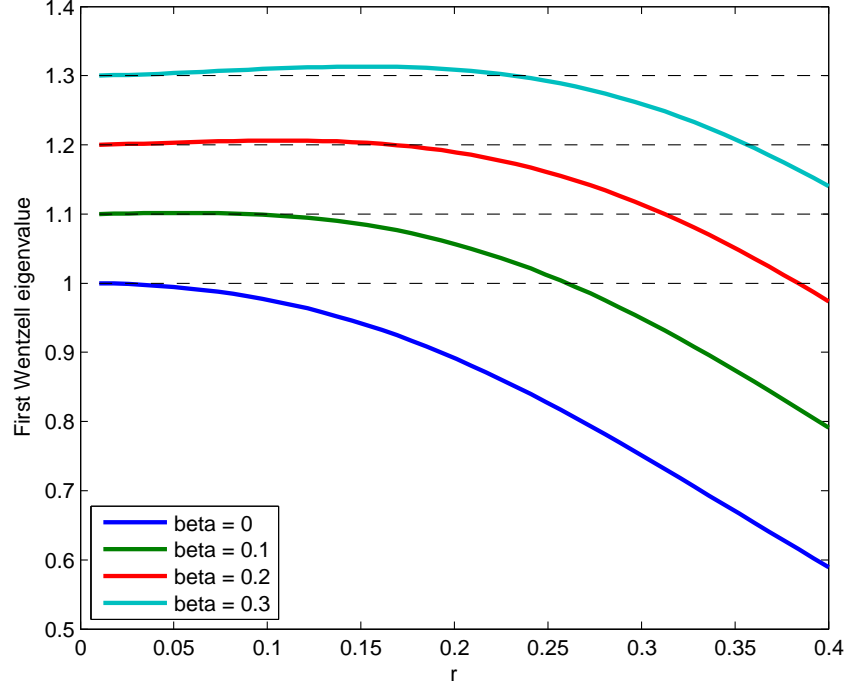


Figure 5: The first Wentzell eigenvalue of the annulus of area π and inner radius r is plotted as a function of r in the cases $\beta = 0, 0.1, 0.2, 0.3$.

6 The FreeFem++ code for solving the Wentzell eigenvalue problem

```

int i;
real t,beta = 2;
// Domain definition using a radial function
border C(t=0,2* pi){x=cos(t)*(1+0.1*cos(t)+0.1*cos(5*t)+
                    0.1*sin(2*t)-0.1*sin(5*t));
                    y=sin(t)*(1+0.1*cos(t)+0.1*cos(5*t)+
                    0.1*sin(2*t)-0.1*sin(5*t));}

mesh Th = buildmesh (C(500));
fespace Vh(Th,P1); // Build P1 finite element space
Vh uh,vh;
// Define the problem via weak formulation
varf va(uh, vh) = int2d(Th) ( dx(uh)*dx(vh)+dy(uh)*dy(vh) )+
                    int1d(Th,1) (beta*(dx(uh)*dx(vh)-
                    dx(uh)*N.x*(N.x*dx(vh)+N.y*dy(vh)) -
                    dx(vh)*N.x*(N.x*dx(uh)+N.y*dy(uh)) +
                    N.x*(dx(vh)*N.x+dy(vh)*N.y)*N.x*(dx(uh)*N.x+dy(uh)*N.y) +
                    dy(uh)*dy(vh) -
                    dy(uh)*N.y*(dx(vh)*N.x+dy(vh)*N.y) -
                    dy(vh)*N.y*(dx(uh)*N.x+dy(uh)*N.y) +
                    (N.y)^2*(dx(vh)*N.x+dy(vh)*N.y)*(dx(uh)*N.x+dy(uh)*N.y) );
varf vb(uh, vh) = int1d(Th,1) (uh * vh);
// Solve the generalized eigenvalue problem
matrix A = va(Vh, Vh ,solver = sparsesolver);
matrix B = vb(Vh, Vh);
real cpu=clock(); // get the clock
int eigCount = 10; // Get first Eigenvalues

```



```

real[int] ev(eigCount); // Holds Eigenfunctions
Vh[int] eV(eigCount); // Holds Eigenfunctions
// Solve Ax=l*Bx
int numEigs = EigenValue(A,B,sym=true,sigma=0,
                        value=ev,vector=eV);
for(int i=0;i<eigCount;i++) // Plot the spectrum
  plot(eV[i],fill=true,value=true,cmm= ev[i]);
cout << " CPU time = " << clock()-cpu << endl;
for(i = 0;i<eigCount;i++)
  cout << ev[i] << endl;

```

7 Laplace-Beltrami eigenvalues of subsets of the sphere

In order to study partitioning problems related to the Laplace-Beltrami eigenvalues, we need to be able to compute efficiently numerical approximations of these eigenvalues on subsets of a surface. We consider here the particular case the sphere. Motivated by the fact that the Laplace-Beltrami eigenvalues for a closed curve in \mathbb{R}^2 can be found using fundamental solutions, as seen in previous sections, we extend the method to the case of the unit sphere in \mathbb{R}^3 . In order to do this we consider the extended problem

$$\begin{cases} -\Delta_\tau u = \lambda u & \text{on } \mathbb{S}^2 \\ -\Delta u = 0 & \text{in a neighborhood of } \mathbb{S}^2. \end{cases} \quad (8)$$

The motivation behind this consideration is the following decomposition of the Laplacian

$$\Delta u = \Delta_\tau u + \mathcal{H} \frac{\partial u}{\partial n} + \frac{\partial^2 u}{\partial n^2}, \quad (9)$$

which reduces the study of the Laplace-Beltrami operator to the study of the normal derivatives of order 1 and 2. For a proof of (9) and more details we refer to [30]. As usual, \mathcal{H} denotes the mean curvature of the surface. We denote $\frac{\partial^2 u}{\partial n^2} = (D^2 n \cdot u) \cdot u$.

As before, we seek u as a linear combination of radial harmonic functions in \mathbb{R}^3 which do not have singularities on \mathbb{S}^2 . We consider the fundamental solution of the Laplace equation in three dimensions given by $\phi(x) = 1/|x|$. We choose a family of N evaluation points (x_i) on \mathbb{S}^2 which are uniformly distributed. We can do an explicit construction starting from a dodecahedron in the case of the sphere, or we can use DistMesh [34] in general situations. The source points (y_i) are chosen on the normals at \mathbb{S}^2 at x_i at a fixed distance r to the center of the sphere. We may choose the source points inside the sphere ($r < 1$) or outside the sphere ($r > 1$). As we will see below, the behaviour of the error depends on r and N . These parameters should be chosen such that the matrices involved in the computations are well conditioned. In the case of the sphere, when considering 600 points, for example, we may choose $r \in [0.5, 0.7] \cup [1.7, 2]$ and we note that the errors tend to get smaller as the source points are far from the surface. This obviously favours the choice of the source points at the exterior of the sphere, which is a choice we make from here on. For each source point y_i we consider the fundamental solution centered in y_i defined by $\psi_i(x) = \phi(|x - y_i|)$. We seek u in the form

$$u = \alpha_1 \psi_{y_1} + \dots + \alpha_N \psi_{y_N}.$$

We impose the eigenvalue condition in each of the points (x_i) and we obtain the equations

$$-\Delta_\tau(\alpha_1 \psi_{y_1}(x_i) + \dots + \alpha_N \psi_{y_N}(x_i)) = \lambda^{LB}(\mathbb{S}^2)(\alpha_1 \psi_{y_1}(x_i) + \dots + \alpha_N \psi_{y_N}(x_i)), \quad i = 1 \dots N. \quad (10)$$

Solving this generalized eigenvalue problem we expect to find the values of the Laplace Beltrami eigenvalues on the unit sphere. The explicit eigenvalues are of the form $\ell(\ell + 1)$ with multiplicity $2\ell + 1$, with $\ell \geq 0$. We recall that r is the distance from the exterior points (y_i) to the center of the sphere. The choice of the sample points (x_i) is not random. As noted in [4], the sample points should be distributed evenly across the surface in order to obtain meaningful results. We tried multiple choices for the points (x_i) :

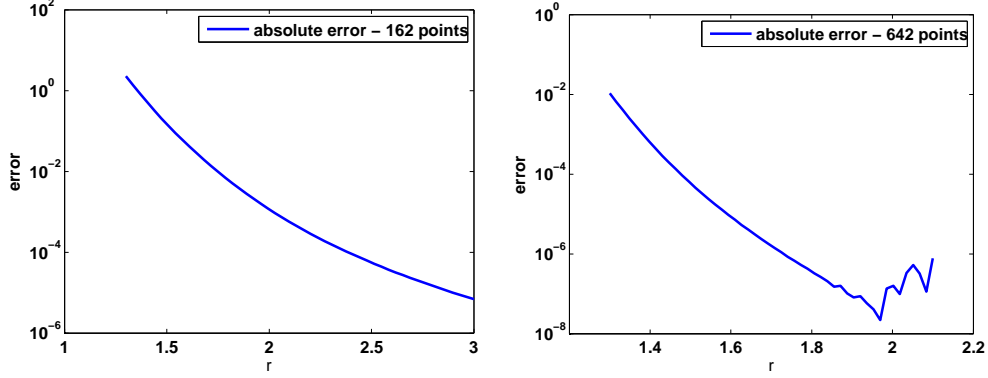


Figure 6: Absolute errors - approximation of the first 10 Laplace-Beltrami eigenvalues of \mathbb{S}^2 .

- uniform sphere mesh found with Distmesh [34],
- the layer method described in [4],
- a uniformly refined mesh of the sphere starting from an icosahedron.

For all these choices of points we observe that the values obtained with our algorithm are very close to the analytical ones. An analysis of the dependence of the absolute error of the parameter r and on the number of sample points is given in Figure 6. These estimates are valid for the first 10 eigenvalues. We can see that the error decreases drastically with r . We also observe that when we have a large number of points and large r there are stability issues in the computation, due to the conditioning of the matrices.

We can adapt the method of fundamental solutions in order to compute the Laplace-Beltrami eigenvalues with Dirichlet boundary conditions of a subset ω of \mathbb{S}^2 . In order to do this we consider only sample points $x_i \in \omega$ and approximate $\lambda^{LB}(\omega)$ using a variation of equation (10). Indeed, let $(x_i)_{i=1}^{N-M}$ be points in the interior of ω (relative to S) and $(z_i)_{i=1}^M$ be points on $\partial\omega$ (relative to S). Using the same method of fundamental solutions, the eigenvalue condition is exactly (10). The boundary conditions can be written as

$$\alpha_1 \psi_{y_1}(z_j) + \dots + \alpha_N \psi_{y_N}(z_j) = 0, \quad j = 1 \dots M. \quad (11)$$

It is possible to couple the systems (10) and (11) into one single generalized eigenvalue problem in the form

$$\begin{pmatrix} A \\ B \end{pmatrix} v = \lambda \begin{pmatrix} X \\ O \end{pmatrix} v \quad (12)$$

where

- $A = (-\Delta_\tau \psi_{y_j}(x_i))$, $i = 1 \dots N - M$, $j = 1 \dots N$
- $B = (\psi_{y_j}(z_k))$, $k = 1 \dots M$, $j = 1 \dots N$
- $X = (\psi_{y_j}(x_i))$, $i = 1 \dots N - M$, $j = 1 \dots N$
- O is the zero matrix of size $(N - M) \times N$.
- $v = (\alpha_1, \dots, \alpha_N)^T$.

The points $(x_i), (z_j)$ are chosen by performing a triangulation of the set $\omega \subset S$, which in our computations will always be a geodesic polygon. In order to compute such a triangulation, we divide the polygon into triangles and then refine this triangulation multiple times by considering the classical midpoint refinement.

In order to test our computational method, we consider some particular subsets of the sphere for which some of the eigenvalues are known explicitly. In the following we call *lens* of angle θ , a portion

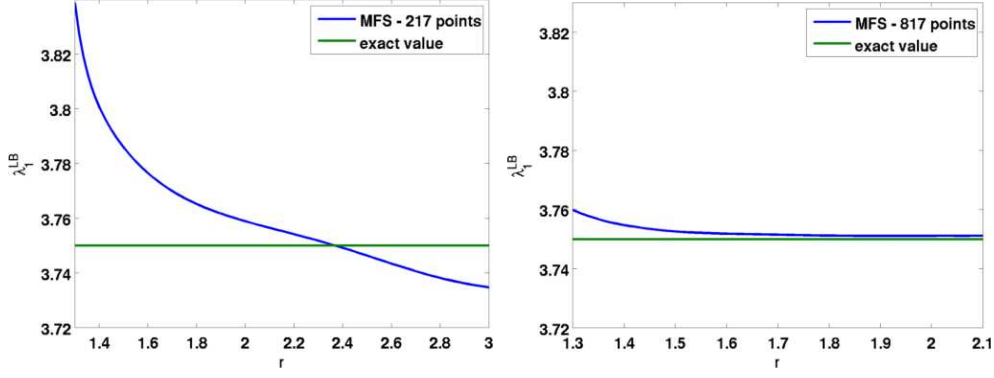


Figure 7: Behavior of the $L(2\pi/3)$ eigenvalue approximation with respect to the parameter r , for 217 and 817 sample points

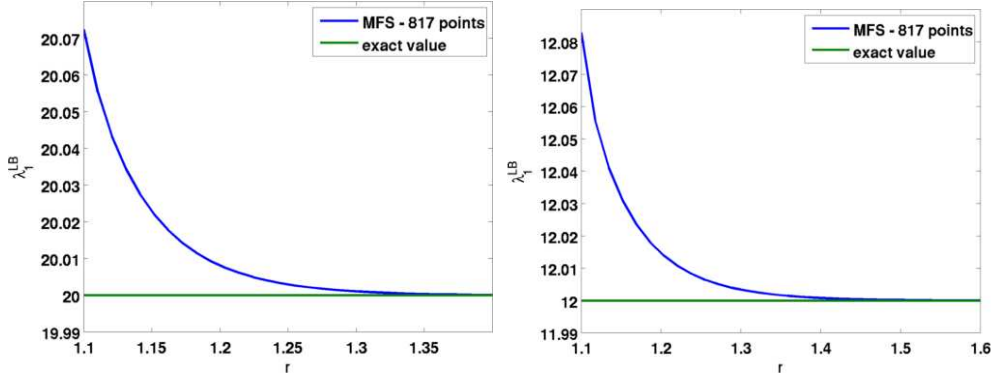


Figure 8: Behavior of the approximation of $R(\pi/3)$ (left) and $R(\pi/2)$ (right) with respect to r

of the sphere contained between two half-meridians which make angle θ . We denote the first eigenvalue of a lens of angle θ by $L(\theta)$. We call a *double-right triangle* of angle θ a half (divided by the ecuatorial circle) of a lens of angle θ . We denote the first eigenvalue of a double-right-triangle of angle θ by $R(\theta)$. The following analytical values are known for $R(\theta)$, $L(\theta)$:

- $L(\theta) = \frac{\pi}{\theta} \left(\frac{\pi}{\theta} + 1 \right)$ (see [40]) - numerical example in Figure 7.
- $R(\pi/3) = 20$, $R(\pi/2) = 12$, $R(\pi) = 6$ (see [40]) - numerical examples in Figure 8)

Another interesting spherical triangle is the one which realizes the partition of the sphere into 4 congruent equilateral triangles. We denote one such triangle by T . The computation of the first eigenvalue of this triangle came up in [39] in the study of the expected capture time of some brownian motion predators on the line. The numerical value computed in the above reference is $\lambda_1^{LB}(T) = 5.1589$ (represented by the green line in Figure 9). We compute numerically this first eigenvalue and compare it to the values presented in the cited article (see Figure 9). We observe that for $r \in [1.8, 1.9]$ the numerically obtained eigenvalues are close to the value mentioned above. We see again the instability in the computation as r increases. In order to further test this numerical value, we used a finite element discretization of the triangle T , and we compute the first eigenvalue in terms of on a mesh having 98000 points. We obtain $\lambda_1^{LB}(T_{fem}) = 5.1593$, which is close to both the result of [39] and our values. We note, though, that in order to reach this precision, more than 50 times more points are needed in the discretization.

Until now we only considered exact subsets of \mathbb{S}^2 . We can extend our method based on fundamental solutions to compute the spectrum associated to an approximation φ of χ_ω . In order to do this, we use the relaxed formulation inspired from [19], [14] given by

$$-\Delta_\tau u + \mu u = \lambda u,$$

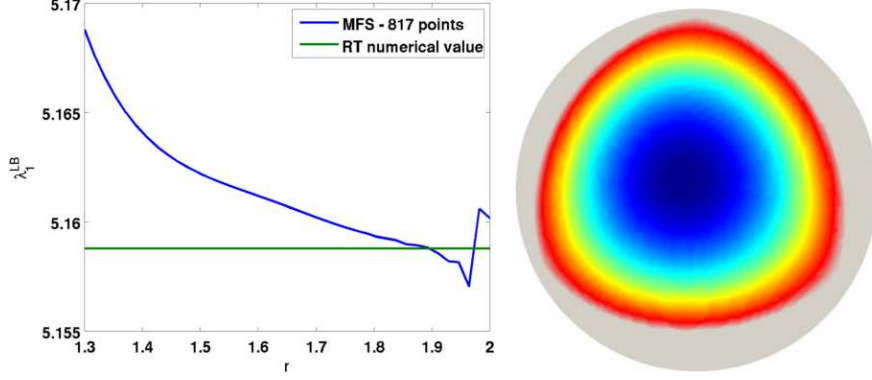


Figure 9: Behavior of the approximate first eigenvalue of T with respect to r (left), corresponding first eigenfunction (right)

where μ is a capacitary measure which penalizes points outside ω . This relaxed formulation includes the classical case. We can compute the eigenvalues of $\omega \subset \mathbb{S}^2$ with Dirichlet boundary condition by imposing $\mu = +\infty$ in $\mathbb{S}^2 \setminus \omega$ and $\mu = 0$ in ω . The advantage is that we work on the whole sphere and the measure μ takes into account the change of shape. This method allows the computation of eigenvalues of different domains by using the same discretization space. In this way it is possible to study partitioning problems which are related to Laplace-Beltrami eigenvalues. The Euclidean case of this problem was considered by Bourdin, Bucur and Oudet in [14], while the spherical case was recently treated by Elliott and Ranner in [22] using a relaxed formulation inspired from [17].

In the computations we choose $\mu = C(1 - \varphi)d\sigma$ and the penalized formulation becomes

$$-\Delta_\tau u + C(1 - \varphi)u = \lambda u. \quad (13)$$

This can be written in matrix form as

$$(A + C \text{diag}(1 - \varphi)B)v = \lambda Bv,$$

where

- $A = (-\Delta_\tau \psi_j(x_i)), i, j = 1 \dots N$
- $B = (\psi_j(x_i)), i, j = 1 \dots N$
- $v = (\alpha_1, \dots, \alpha_N)^T$
- $\text{diag}(1 - \varphi)$ is the diagonal matrix with diagonal entries $1 - \varphi$.

For the generalized eigenvalues computations we use the Matlab `eigs` function. In order to be able to perform an optimization, we need to compute the gradient of the eigenvalue with respect to φ . For this we have two options:

- Compute the gradient in the analytic setting and obtain $\nabla \lambda(\varphi) = -Cv^2$ where v is the associated eigenfunction. This was proved in [14].
- Compute the gradient in the discrete setting, by differentiating the generalized eigenvalue problem. In order to do this, we need the corresponding right eigenvector v and the left eigenvector w . We obtain that

$$\nabla \lambda(\varphi) = -Cw \otimes Bv / (w^T Bv),$$

where \otimes is the pointwise product.

Both of the above methods work well, but the second needs to perform two times the amount of computations as the first, since we need both the left and right corresponding eigenvectors. In our computations we prefer the first approach, as it is faster. The optimization is made using a standard gradient descent algorithm. We need to impose the partition condition at each iteration, and we do this by applying the following projection operator inspired from [14]

$$\Pi(\varphi^l) = \frac{|\varphi^l|}{\sum_{i=1}^n |\varphi^i|}, \quad l = 1, \dots, n.$$

8 Numerical optimal partitions on the sphere

The main motivation for performing numerical computations regarding spectral spherical partitions is the fact that problems that are simple to state regarding these optimal partitions are still open. Bishop proved that the partition of \mathbb{S}^2 into two parts ω_1, ω_2 which minimizes $\lambda_1^{LB}(\omega_1) + \lambda_1^{LB}(\omega_2)$ consists of two half-spheres. The similar problem of finding the minimizer of

$$\lambda_1^{LB}(\omega_1) + \lambda_1^{LB}(\omega_2) + \lambda_1^{LB}(\omega_3), \quad (\omega_1, \omega_2, \omega_3) \text{ partition of } \mathbb{S}^2,$$

is open. In the same article [9] it is conjectured that the optimal partition in the case $n = 3$ consists of three $2\pi/3$ -lens, the so-called Y partition. A similar problem, which less strong than Bishop's conjecture, was treated by Helffer et al. in [29]. They proved that the partition of the sphere into three $2\pi/3$ -lens minimizes the quantity

$$\max_{i=1,2,3} \lambda_1^{LB}(\omega_i), \quad (\omega_1, \omega_2, \omega_3) \text{ partition of } \mathbb{S}^2.$$

We recall that numerical evidence of the validity of Bishop's conjecture was presented in [38]. A more detailed numerical study of the optimal spectral partitions on \mathbb{S}^2 was performed by Elliott and Ranner in [22]. The authors confirm numerically Bishop's conjecture and they present computations for partitions having $n = 3, 4, 5, 6, 7, 8, 16, 32$ components. Their method is based on a penalized energy formulation of the partitioning problem introduced in [16]. Instead of minimizing the sum of eigenvalues they choose to minimize the energy

$$\mathcal{E}_\varepsilon(u) = \sum_{i=1}^n \frac{1}{2} \int_{\mathbb{S}^2} |\nabla u_i|^2 + \frac{1}{\varepsilon^2} \sum_{i=1}^n \sum_{j=1, j \neq i}^n \int_{\mathbb{S}^2} u_i^2 u_j^2.$$

where $\|u_i\|_{L^2(\mathbb{S}^2)} = 1$. The optimal energies presented in [22] are computed using this relaxed formulation. It is natural to see that as soon as ε is positive the optimal energy $\min \mathcal{E}_\varepsilon(u)$ is lower than the actual sum of eigenvalues. Indeed, we see that for ε positive the supports of the approximated eigenfunctions u_i may overlap, and thus the corresponding eigenvalues are lower. On the other hand the values computed with our method tend to be greater or equal to the actual eigenvalues, and therefore the optimal costs obtained with our computational method are always greater than the costs presented in [22].

In the following, we propose the use of a different approach, inspired by the two dimensional case studied by Bourdin, Bucur and Oudet [14]. We represent each phase ω_i of the partition by a density function $\varphi_i : \mathbb{S}^2 \rightarrow [0, 1]$. The partition condition then translates to $\sum_{i=1}^n \varphi_i = 1$. Given φ , a density function approximating ω , we consider the problem

$$-\Delta_\tau u + C(1 - \varphi)u = \lambda_1^{LB}(C, \varphi)u \text{ on } \mathbb{S}^2 \quad (14)$$

with $C \gg 1$. As in [14], it can be proved that the mapping $\varphi \mapsto \lambda_1^{LB}(C, \varphi)$ is concave and we have $\lambda_1^{LB}(C, \chi_\omega) \rightarrow \lambda_1^{LB}(\omega)$ as $C \rightarrow \infty$.

We were able to compute numerically the optimal partitions for

$$\sum_{i=1}^n \lambda_1^{LB}(\omega_i), \quad (\omega_1, \dots, \omega_n) \text{ partition of } \mathbb{S}^2,$$

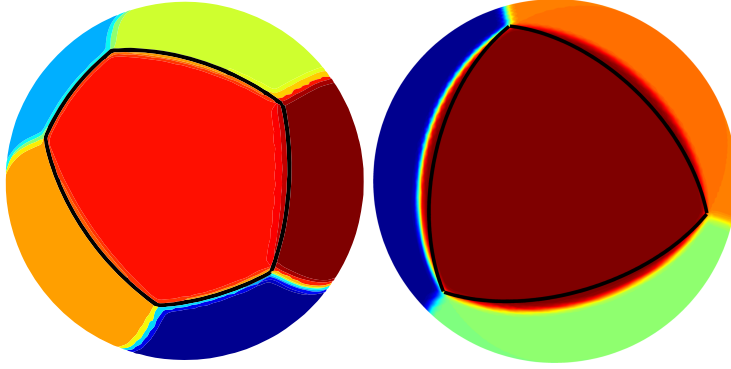


Figure 10: The optimal configuration for $n = 8$ (left) and $n = 5$ (right). The black lines are geodesic arcs connecting the vertices of a face.

for $n \in [3, 24] \cup \{32\}$, using about 5000 sample points. It is interesting to note that for $n \in \{3, 4, 6, 12\}$ we obtain the regular tiling of the sphere. For $n \in \{5, 7, 8, 32\}$ we obtain the same results as Elliott and Ranner. For $n = 16$ we obtain something slightly different: we obtain 4 equal hexagons centred at the vertices of a regular tetrahedron and 12 equal pentagons linking them. Elliott and Ranner obtained a configuration of 4 equal hexagons, 4 equal pentagons and another 8 equal pentagons. We have also obtained a similar configuration as a local minimum. The cost associated to the Elliott Ranner configuration, computed with our method, is 374.68 compared to our optimal configuration which has a lower cost of 371.76. You can see two views of the corresponding partitions in Figure 11.

In [22] it is conjectured that the common boundary of two adjacent cells is a geodesic arc. In Figure 10 we plotted some geodesic arcs on top of the results obtained using density functions. We can observe that indeed, for $n = 8$ the boundaries of the cells are close to geodesic arcs. On the other hand, for $n = 5$ we see an obvious non-overlapping of the geodesics and the boundaries. In order to test the validity of this conjecture we propose the following **optimization procedure**.

- We perform the optimization using the penalized method inspired from [14] starting from random densities on the sphere. This first step gives us the approximations of the characteristic functions of the optimal configuration.
- In a second step we detect the polygonal structure of the partition and we assume that every edge connecting two vertices of these polygons is a geodesic arc. We take the vertices of the polygons as variables and we find the optimal partition in the class of geodesic polygons. At this stage we compute the eigenvalue of each cell using the method of fundamental solutions described in the previous section.
- Once we obtain the optimal configuration among geodesic polygons, we enrich the class of domains by adding midpoints of the arcs as new variables. We perform the optimization in this new class and we see if the value of the optimal cost decreases.

In order to perform the second step, the optimization in the class of geodesic polygons, we extract the topological structure from the optimal densities (points, edges and faces connectivities). For each polygon in the partition we compute the corresponding first eigenvalue using the method presented in (12). We search the position of the triple points, which are the only variables here, for which we have the least sum of first eigenvalues. It is possible to perform this optimization with the following algorithm:

- For each point P consider a family of q tangential directions $(v_i)_{i=1}^q$ chosen as follows: the first direction is chosen randomly and the rest are chosen so that the angles between consecutive directions are $2\pi/q$.
- Evaluate the cost function for the new partition obtained by perturbing the point P in each of the directions v_i according to a parameter ε .

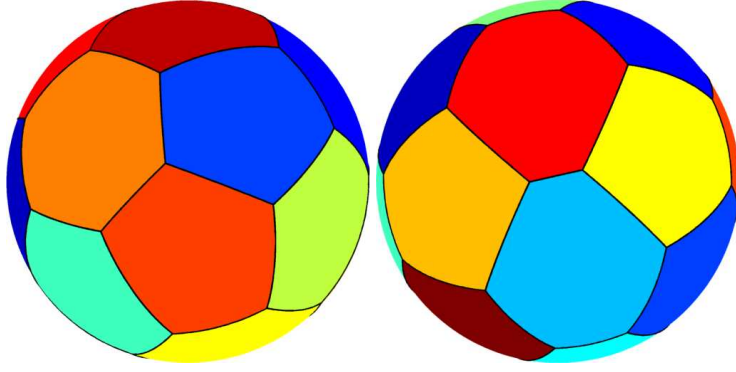


Figure 11: Our candidate for $n = 16$ (left): four regular hexagons centered in the vertices of a regular tetrahedron, linked by 12 equal pentagons. The corresponding cost is 371,76. The candidate obtained by Elliott and Ranner (right): two pairs of hexagons connected by three types of pentagons. The corresponding cost is 374.68

n	Geodesics	Enriched class	Cost decrease
5	34.46	34.42	0.04
7	68.99	68.97	0.02
8	90.97	90.92	0.05
9	115.12	115.08	0.04
10	143.25	143.20	0.05

Table 5: Illustration of cost decrease after adding midpoints as variables

- Choose the direction which has the largest decrease, and this is the updated partition.
- If there is no decrease for each of the points of the partition, then decrease ε .

This algorithm converges and its accuracy has been tested by choosing different starting configurations, and observing that it always converges to the same partition. The optimal densities and the optimal partitions consisting of geodesic polygons are presented in figures that can be found at the end of this section. The optimal costs are computed using the method of fundamental solutions. We present the results obtained in the cases corresponding to $n \in \{3, 4, \dots, 16, 20, 32\}$. Computations were made for $n \in \{17, 18, 19, 21, 22, 23, 24\}$, but the presentation of the corresponding figures does not present any particular interest.

To illustrate the third stage of the optimization, we give more details concerning the case $n = 5$. The optimal partition into geodesic polygons consists of two triangles and four rectangles. Adding the midpoints as variables gives us a new configuration of two hexagons and three octagons. What we observed in the case $n = 5$ is that adding midpoints as additional degrees of freedom brings us to a new partition with smaller optimal cost. For $n = 5$ we obtain a decrease of 0.04 in the optimal cost value. The same procedure applied for $n = 7$ allows us to decrease the optimal value with 0.02. These two cases are presented in Figure 12. This simple numeric observation suggests that the boundaries of the cells in a minimal configuration are not necessarily geodesic arcs. We performed the same algorithm in the cases $n \in \{8, 9, 10\}$. We summarize the results in Table 5.

We can present another argument which shows that, given the numerical results in cases $n = 11$ and $n \geq 13$, there are cells whose boundaries are not geodesics. We recall that for a subset M of a smooth surface with piecewise smooth boundary, the Gauss-Bonnet formula says that

$$\int_M K dA + \int_{\partial M} k_g + \sum \theta_i = 2\pi\chi(M), \quad (15)$$

where K is the curvature of the surface, k_g is the geodesic curvature of ∂M , θ_i are the turning angles in the vertices and $\chi(M)$ is the Euler characteristic of M , which is equal to 1 in the case of a geodesic

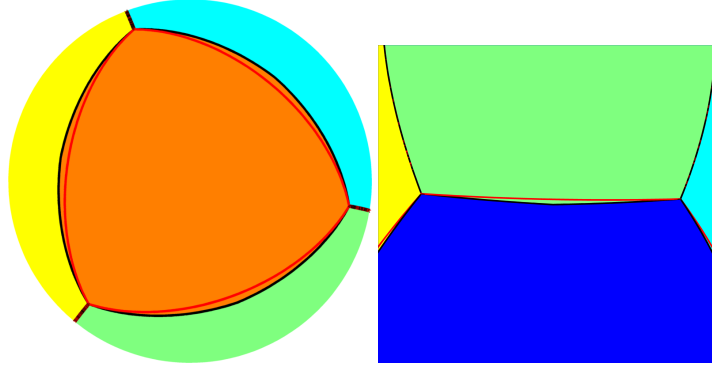


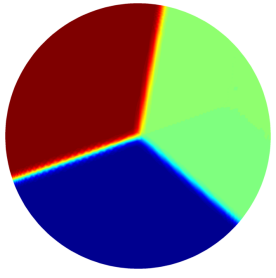

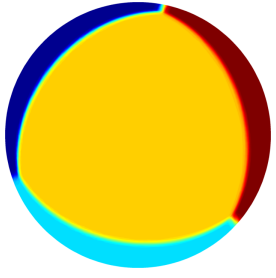
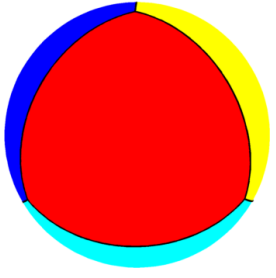
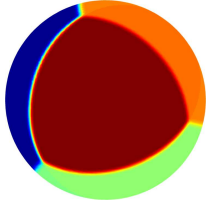
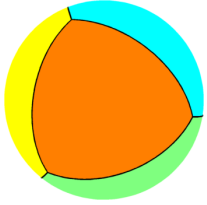
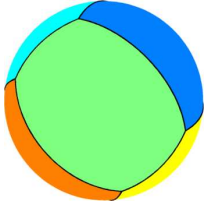
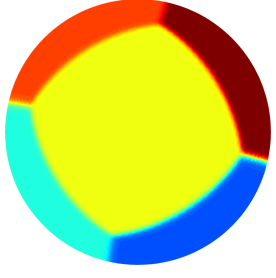
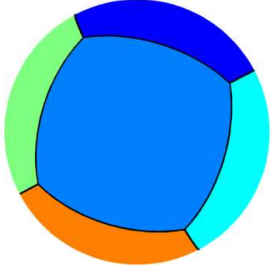
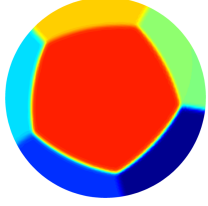
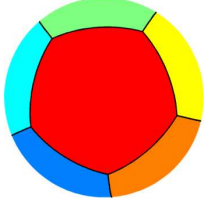
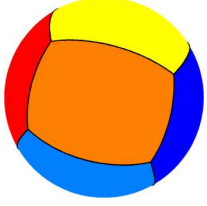
Figure 12: The study of the cases $n \in \{5, 7\}$; the regions correspond to the non-geodesic optimal partition and the red arcs are geodesics. Adding midpoints as variables reduces the value from 34.46 to 34.42 for $n = 5$ and from 68.99 to 68.97 for $n = 7$.

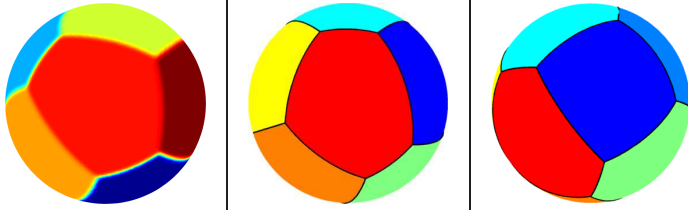
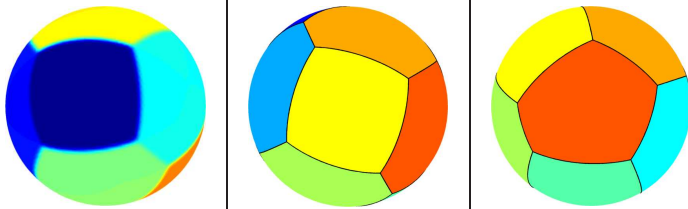
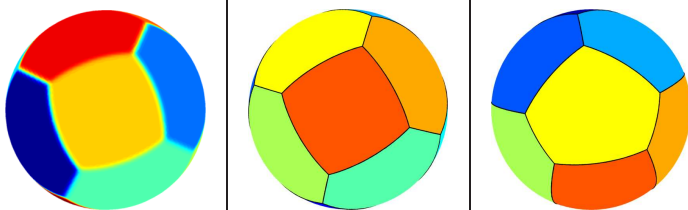
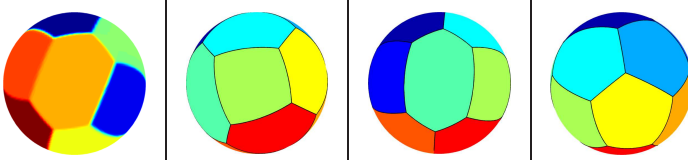
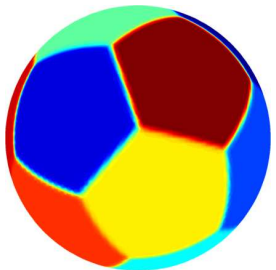
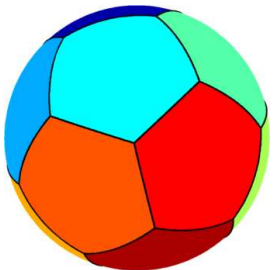
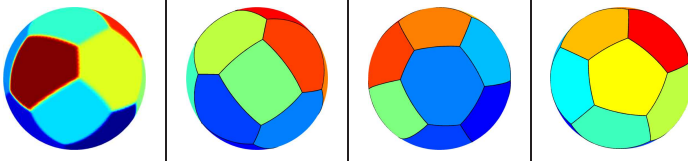
polygon. We refer to [21] for further details regarding this theorem. Let's suppose that the boundaries of the optimal partition are geodesics and that the partition contains a hexagonal domain. The optimality conditions proved in [18] imply that at all polygonal regions in the optimal configuration have angles with measure $2\pi/3$. A simple application of the Gauss-Bonnet's formula implies that geodesic hexagons on the sphere which have all angles equal to $2\pi/3$ have area zero. Thus no hexagonal domain in the optimal configuration can have boundary formed only of geodesics. As a conclusion of this fact and of our computations, for $n = 11$ and $n \geq 13$ the boundaries of the cells are not all geodesics.

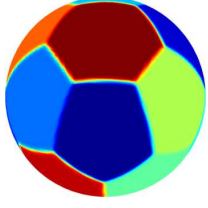
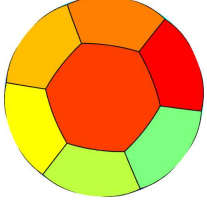
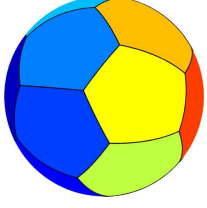
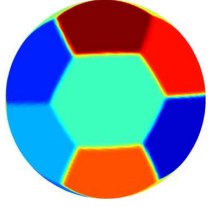
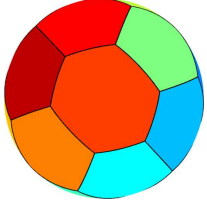
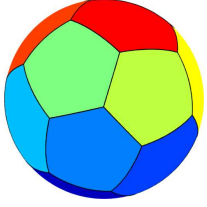
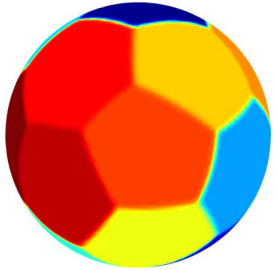
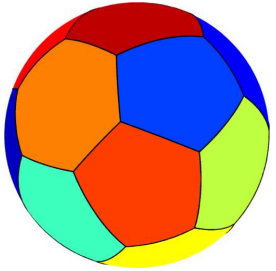
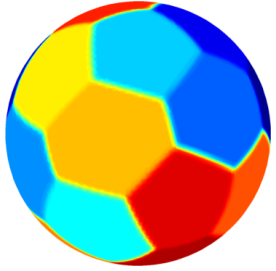
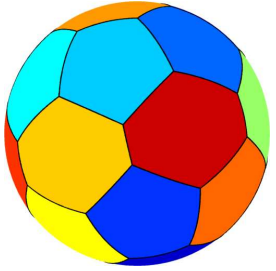
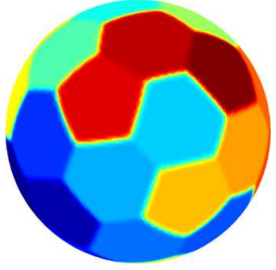
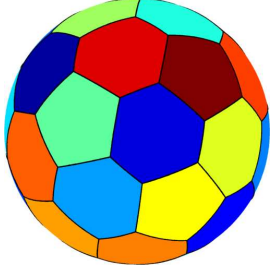
Discussion of the results.

- We observe that for $n \in \{4, 6, 12\}$ the optimal partition cells are regular geodesic polygons corresponding to the tetrahedron, the cube and the dodecahedron. For $n = 3$ we obtain the expected Y partition which confirms numerically Bishop's conjecture.
- We remark the fact that for $n \geq 14$ optimal partitions seem to consist of 12 pentagons and $n - 12$ hexagons. We notice that except in cases $n \in \{11, 13\}$ there seem to be only two types of polygons in the optimal partition.
- The third stage in the optimization procedure suggested above and the argument based on Gauss-Bonnet formula allows us to deduce that, in general, except the cases $n = 3, 4, 6, 12$, the boundaries of the optimal cells are probably not geodesic arcs.

An equally interesting problem is finding the partition which minimizes the quantity $\max_i \lambda_1^{LB}(\omega_i)$. Theoretical aspects of the problem as well as a complete analysis of the case $n = 3$ were given in [29]. It is known that if the solution of the problem corresponding to the sum consists of cells with the same eigenvalue, then this is also a solution of the maximum problem. In our computations, only the regular partitions corresponding to $n \in \{3, 4, 6, 12\}$ have this property and thus they are good candidates as optimizers for the maximum problem as well. In all remaining cases we obtained at least two cells with different eigenvalues, which means that our partitions cannot be optimal for the min-max problem. Optimizing the maximum is not straightforward since we are dealing with a non-differentiable functional. Following the approach in [13], we may expect that minimizing a p -norm for high p will get us close to the optimal partition for the maximum. Some experiments done in this direction indicate that the topology of the optimal partition for the maximum is the same as the one for the sum, but the boundaries are just slightly moved in order to have the same eigenvalue for every one of the cells.

<p>$n = 3$: three 120° lens. Confirmation of the conjecture proposed by Bishop [9]. optimal cost = $45/4$ lens eigenvalue = $15/4$.</p>			
<p>$n = 4$: the optimal partition consists of the tiling generated by a regular tetrahedron inscribed in the sphere. optimal cost = 20.635 triangle eigenvalue = 5.1588</p>			
<p>$n = 5$: two equal equilateral triangles and three equal rectangles. optimal cost = 34.46. triangle eigenvalue = 7.35 rectangle eigenvalue = 6.58.</p>			
<p>$n = 6$: regular tiling generated by the cube optimal cost = 48.6. square eigenvalue = 8.10</p>			
<p>$n = 7$: two regular pentagons and 5 equal rectangles. optimal cost = 68.99. pentagon eigenvalue = 8.61 rectangle eigenvalue = 10.35.</p>			

<p>$n = 8$: four equal quadrilaterals and four equal pentagons. optimal cost = 90.97. pentagon eigenvalue = 10.80 quadrilateral eigenvalue = 11.94.</p>				
<p>$n = 9$: 3 equal squares and 6 equal pentagons. optimal cost = 115.12. square eigenvalue = 13.65 pentagon eigenvalue = 12.36.</p>				
<p>$n = 10$: two equal squares and 8 equal pentagons optimal cost = 143.25. square eigenvalue = 15.85 pentagon eigenvalue = 13.94.</p>				
<p>$n = 11$: one hexagon, two equal quadrilaterals, eight pentagons of three types optimal cost = 175.34.</p>				
<p>$n = 12$: regular tiling generated by the dodecahedron optimal cost = 203.71. pentagon eigenvalue = 16.98</p>				
<p>$n = 13$: one rectangle, two equal hexagons, 10 pentagons of three types optimal cost = 245.37.</p>				

<p>$n = 14$: two equal hexagons and 12 equal pentagons optimal cost = 283.59. hexagon eigenvalue = 17.34 pentagon eigenvalue = 20.74.</p>			
<p>$n = 15$: 3 equal hexagons and 12 pentagons of two types optimal cost = 327.21.</p>			
<p>$n = 16$: 4 equal hexagons and 12 equal pentagons optimal cost = 371.76.</p>			
<p>$n = 20$: 8 hexagons and 12 pentagons optimal cost = 585.75.</p>			
<p>$n = 32$: 20 equal hexagons and 12 equal pentagons optimal cost = 1504.16.</p>			

9 Conclusions

The method of fundamental solutions seems to be well adapted to the study of the boundary eigenvalue problems corresponding to the Steklov, Wentzell and Laplace-Beltrami operators. The numerical methods presented in this article have good properties regarding their accuracy and speed. This behaviour encourages their use in the study of shape optimization problems. The computation of the Steklov or

Wentzell spectrum is very fast and precise in the case where the boundary of the domain is regular enough. It is true that the applicability is restricted to simply connected domains which do not have cusps. We were able to confirm numerically the conjecture regarding the optimality of the disk for the first Wentzell eigenvalue proposed in [20].

The method based on fundamental solutions is proved useful in the study of the spectral partitions on manifolds. We are able to obtain results similar to [22] and we also can confirm Bishop's conjecture regarding the optimality of the Y partition of the sphere (we recall that evidence of the validity of this conjecture can also be found in [38] and [22]). The numerical computations suggest that for $n \in \{4, 6, 12\}$ the optimal partition is the one associated to the corresponding regular polyhedron. The numerical study made for $n \in \{5, 7, 8, 9, 10\}$ and suggests that boundaries are not all geodesics in this case. A simple argument based on the Gauss-Bonnet formula proves that as soon as there is a hexagonal domain in the optimal configurations, its boundary is not formed of geodesic arcs. In conclusion, a part from the cases $n \in \{3, 4, 6, 12\}$ the optimal configuration is not made of geodesic polygons.

Acknowledgements

Bishop's conjecture was brought to our knowledge by Bernard Helffer. The author wishes to thank him for the stimulating discussions we had concerning the numerical study of spectral partitions.

References

- [1] E. Akhmetgaliyev, C.-Y. Kao, and B. Osting. Computational methods for extremal steklov problems, 2016.
- [2] C. J. S. Alves and P. R. S. Antunes. The method of fundamental solutions applied to the calculation of eigensolutions for 2D plates. *Internat. J. Numer. Methods Engrg.*, 77(2):177–194, 2009.
- [3] C. J. S. Alves and P. R. S. Antunes. The method of fundamental solutions applied to some inverse eigenproblems. *SIAM J. Sci. Comput.*, 35(3):A1689–A1708, 2013.
- [4] P. R. S. Antunes. Numerical calculation of eigensolutions of 3D shapes using the method of fundamental solutions. *Numer. Methods Partial Differential Equations*, 27(6):1525–1550, 2011.
- [5] P. R. S. Antunes. Optimization of sums and quotients of Dirichlet-Laplacian eigenvalues. *Appl. Math. Comput.*, 219(9):4239–4254, 2013.
- [6] P. R. S. Antunes and P. Freitas. Numerical optimization of low eigenvalues of the Dirichlet and Neumann Laplacians. *J. Optim. Theory Appl.*, 154(1):235–257, 2012.
- [7] C. Bandle. *Isoperimetric inequalities and applications*, volume 7 of *Monographs and Studies in Mathematics*. Pitman (Advanced Publishing Program), Boston, Mass.-London, 1980.
- [8] A. H. Barnett and T. Betcke. Stability and convergence of the method of fundamental solutions for Helmholtz problems on analytic domains. *J. Comput. Phys.*, 227(14):7003–7026, 2008.
- [9] C. J. Bishop. Some questions concerning harmonic measure. In *Partial differential equations with minimal smoothness and applications (Chicago, IL, 1990)*, volume 42 of *IMA Vol. Math. Appl.*, pages 89–97. Springer, New York, 1992.
- [10] B. Bogosel. The steklov spectrum on moving domains. *Appl. Math. Optim.*, 2015.
- [11] B. Bogosel, D. Bucur, and A. Giacomini. On optimal shapes maximizing the steklov eigenvalues. 2016.

- [12] V. Bonnaillie-Noël, B. Helffer, and G. Vial. Numerical simulations for nodal domains and spectral minimal partitions. *ESAIM Control Optim. Calc. Var.*, 16(1):221–246, 2010.
- [13] V. Bonnaillie-Nol and C. Lna. Spectral minimal partitions for a family of tori, 2015.
- [14] B. Bourdin, D. Bucur, and É. Oudet. Optimal partitions for eigenvalues. *SIAM J. Sci. Comput.*, 31(6):4100–4114, 2009/10.
- [15] F. Brock. An isoperimetric inequality for eigenvalues of the Stekloff problem. *ZAMM Z. Angew. Math. Mech.*, 81(1):69–71, 2001.
- [16] L. A. Caffarelli and F.-H. Lin. Singularly perturbed elliptic systems and multi-valued harmonic functions with free boundaries. *J. Amer. Math. Soc.*, 21(3):847–862, 2008.
- [17] L. A. Cafferelli and F. H. Lin. An optimal partition problem for eigenvalues. *J. Sci. Comput.*, 31(1-2):5–18, 2007.
- [18] M. Conti, S. Terracini, and G. Verzini. An optimal partition problem related to nonlinear eigenvalues. *J. Funct. Anal.*, 198(1):160–196, 2003.
- [19] G. Dal Maso and U. Mosco. Wiener’s criterion and Γ -convergence. *Appl. Math. Optim.*, 15(1):15–63, 1987.
- [20] M. Dambrine, D. Kateb, and J. Lamboley. An extremal eigenvalue problem for the Wentzell-Laplace operator. *ArXiv e-prints*, Jan. 2014.
- [21] M. P. do Carmo. *Differential geometry of curves and surfaces*. Prentice-Hall, Inc., Englewood Cliffs, N.J., 1976. Translated from the Portuguese.
- [22] C. M. Elliott and T. Ranner. A computational approach to an optimal partition problem on surfaces, 2014.
- [23] L. C. Evans and R. F. Gariepy. *Measure theory and fine properties of functions*. Studies in Advanced Mathematics. CRC Press, Boca Raton, FL, 1992.
- [24] A. Girouard and I. Polterovich. On the Hersch-Payne-Schiffer estimates for the eigenvalues of the Steklov problem. *Funktsional. Anal. i Prilozhen.*, 44(2):33–47, 2010.
- [25] A. Girouard and I. Polterovich. Spectral geometry of the steklov problem, 2014.
- [26] F. Hecht. New development in FreeFem++. *J. Numer. Math.*, 20(3-4):251–265, 2012.
- [27] B. Helffer, T. Hoffmann-Ostenhof, and S. Terracini. Nodal domains and spectral minimal partitions. *Ann. Inst. H. Poincaré Anal. Non Linéaire*, 26(1):101–138, 2009.
- [28] B. Helffer, T. Hoffmann-Ostenhof, and S. Terracini. Nodal minimal partitions in dimension 3. *Discrete Contin. Dyn. Syst.*, 28(2):617–635, 2010.
- [29] B. Helffer, T. Hoffmann-Ostenhof, and S. Terracini. On spectral minimal partitions: the case of the sphere. In *Around the research of Vladimir Maz’ya. III*, volume 13 of *Int. Math. Ser. (N. Y.)*, pages 153–178. Springer, New York, 2010.
- [30] A. Henrot and M. Pierre. *Variation et optimisation de formes*, volume 48 of *Mathématiques & Applications (Berlin) [Mathematics & Applications]*. Springer, Berlin, 2005. Une analyse géométrique. [A geometric analysis].
- [31] J. Hersch, L. E. Payne, and M. M. Schiffer. Some inequalities for Stekloff eigenvalues. *Arch. Rational Mech. Anal.*, 57:99–114, 1975.

- [32] V. D. Kupradze and M. A. Aleksidze. The method of functional equations for the approximate solution of certain boundary-value problems. *Ž. Vychisl. Mat. i Mat. Fiz.*, 4:683–715, 1964.
- [33] C. B. Moler and L. E. Payne. Bounds for eigenvalues and eigenvectors of symmetric operators. *SIAM J. Numer. Anal.*, 5:64–70, 1968.
- [34] P. olof Persson and G. Strang. A simple mesh generator in matlab. *SIAM Review*, 46, 2004.
- [35] B. Osting. Optimization of spectral functions of Dirichlet-Laplacian eigenvalues. *J. Comput. Phys.*, 229(22):8578–8590, 2010.
- [36] B. Osting and C.-Y. Kao. Minimal convex combinations of sequential Laplace-Dirichlet eigenvalues. *SIAM J. Sci. Comput.*, 35(3):B731–B750, 2013.
- [37] B. Osting and C.-Y. Kao. Minimal convex combinations of three sequential Laplace-Dirichlet eigenvalues. *Appl. Math. Optim.*, 69(1):123–139, 2014.
- [38] B. Osting, C. D. White, and É. Oudet. Minimal Dirichlet energy partitions for graphs. *SIAM J. Sci. Comput.*, 36(4):A1635–A1651, 2014.
- [39] J. Ratzkin and A. Treibergs. A capture problem in Brownian motion and eigenvalues of spherical domains. *Trans. Amer. Math. Soc.*, 361(1):391–405, 2009.
- [40] H. Walden and R. B. Kellogg. Numerical determination of the fundamental eigenvalue for the Laplace operator on a spherical domain. *J. Engrg. Math.*, 11(4):299–318, 1977.
- [41] R. Weinstock. Inequalities for a classical eigenvalue problem. *J. Rational Mech. Anal.*, 3:745–753, 1954.